**ISTANBUL TECHNICAL UNIVERSITY ★ GRADUATE SCHOOL**

# INVESTIGATION OF THE STRUCTURAL AND MECHANICAL PROPERTIES OF THE SINGLE CRYSTAL CMSX-4 SLS SUPERALLOY EXPOSED TO HIGH TEMPERATURE FOR LONG TERM

**M.Sc. THESIS**

**Sertaç ALPTEKİN**

**Department of Metallurgical and Materials Engineering**

**Materials Engineering Programme**

**JUNE 2021**

ISTANBUL TECHNICAL UNIVERSITY ★ GRADUATE SCHOOL

# INVESTIGATION OF THE STRUCTURAL AND MECHANICAL PROPERTIES OF THE SINGLE CRYSTAL CMSX-4 SLS SUPERALLOY EXPOSED TO HIGH TEMPERATURE FOR LONG TERM

**M.Sc. THESIS**

**Sertaç ALPTEKİN**
**(506171439)**

**Department of Metallurgical and Materials Engineering**

**Materials Engineering Programme**

**Thesis Advisor: Prof. Dr. Hüseyin ÇİMENOĞLU**

**JUNE 2021**

**ISTANBUL TEKNİK ÜNİVERSİTESİ ★ LİSANSÜSTÜ EĞİTİM ENSTİTÜSÜ**

# YÜKSEK SICAKLIĞA UZUN SÜRELİ MARUZ BIRAKILAN TEK KRİSTAL CMSX-4 SLS SÜPERALAŞIMIN YAPISAL VE MEKANİK ÖZELLİKLERİNİN İNCELENMESİ

**YÜKSEK LİSANS TEZİ**

**Sertaç ALPTEKİN**
**(506171439)**

**Metalurji ve Malzeme Mühendisliği Anabilim Dalı**

**Malzeme Mühendisliği Programı**

**Tez Danışmanı: Prof. Dr. Hüseyin ÇİMENOĞLU**

**HAZİRAN 2021**

Sertaç Alptekin, a M.Sc. student of İTU Graduate School of Science Engineering and Technology student ID 506171439, successfully defended the thesis/dissertation entitled "INVESTIGATION OF THE STRUCTURAL AND MECHANICAL PROPERTIES OF THE SINGLE CRYSTAL CMSX-4 SLS SUPERALLOY EXPOSED TO HIGH TEMPERATURE FOR LONG TERM", which he prepared after fulfilling the requirements specified in the associated legislations, before the jury whose signatures are below.

| | | |
|---|---|---|
| **Thesis Advisor :** | **Prof. Dr. Hüseyin ÇİMENOĞLU**<br>İstanbul Technical University | .............................. |
| **Jury Members :** | **Prof. Dr. Murat BAYDOĞAN**<br>Istanbul Technical University | ............................. |
| | **Prof. Dr. Erdem ATAR**<br>Gebze Technical University | .............................. |

**Date of Submission : 09/06/2021**
**Date of Defense : 25/06/2021**

*To all my loved ones,*

# FOREWORD

This thesis was a part of “5155A10-Development of Nickel Based Superalloy Materials and Production Processes in Aerospace Applications” project of TÜBİTAK MRC-Materials Institute, Critical Metallic Materials Group which is supported and financed by “Presendency of Defence Industries” (SSB) of Turkey and Tusas Engine Industries Inc-TEI (as contractor and project partner).

First, I am so much grateful to my supervisor Prof. Dr. Hüseyin ÇİMENOĞLU for his valuable supports, supervision, and guidance during my study. He has enlightened me with their practical and scientific knowledge whenever I faced with a problem during my study.

I would like to show my appreciation to Assoc. Prof. Dr. Havva Kazdal ZEYTİN, group leader of Critical Metallic Materials, for her permanent encouragement and support in every step that I take in my study and professional career.

I would like to express my sincere thanks to TÜBİTAK Marmara Research Center Critical Metallic Materials Group members for their dynamic support and help in every step of this thesis. I must also thank to Arda İNCEYER from Gebze Technical University for his help in SEM analysis.

Last but not least, I would like show greatest gratitude to my mom Elif ALPTEKİN and my father Necati ALPTEKİN for their endless support, devotion and guidance during my entire life. They are also very patient with me and always made me feel like they were my side in every step of my life.

Finally, I am so much thankful to Leyla Elif ATAÇ for her patience, endless motivation and kindness. I have always felt her love from deep in my heart.

June 2021

Sertaç ALPTEKİN
Metallurgical and Materials Engineer

## TABLE OF CONTENTS

**Page**

## ABBREVIATIONS

| | |
|---|---|
| **AS-HT** | **:** As-heat treated |
| **AVG** | **:** Average |
| **DS** | **:** Directional solidification |
| **FCC** | **:** Face centrede cubic |
| **IC** | **:** Investment casting |
| **SEM** | **:** Scanning electron microscope |
| **SX** | **:** Single crystal |
| **TCP** | **:** Topologically Closed Packed |
| **TEM** | **:** Transmission electron microscope |
| **TUBITAK MRC** | **:** Marmara research center of The Scientific and Technological Research Council of Turkey |
| **VIM** | **:** Vacuum Induction Melting |
| **XRD** | **:** X-ray diffraction |

## SYMBOLS

**γ** : Gamma phase
**γ’** : Gamma prime phase
**σ** : Sigma phase
**μ** : Mu phase

# LIST OF TABLES

## LIST OF FIGURES

**Page**

# INVESTIGATION OF THE STRUCTURAL AND MECHANICAL PROPERTIES OF THE SINGLE CRYSTAL CMSX-4 SLS SUPERALLOY EXPOSED TO HIGH TEMPERATURE FOR LONG TERM

## SUMMARY

Nickel based superalloys are most popular and preffered materials used in gas turbine engines in aviation industry due to its high stability and mechanical properties at high temperatures. Single crystal (SX) nickel based supealloys are generally used in production of turbine blades in turbine chamber. And they are produced with special casting processes and technologies which consist of controlled solidification and aging heat treatment under vacuum. The most common used SX alloy is called as CMSX-4 alloy.

In this master thesis, the main purpose was investigation and understanding of high temperature behaviour of the SX superalloy. In accordance with this purpose, test bars were first casted and solidified in <001> direction as single crytal form meaning that no grain boundaries exist in the structure by using investment casting technique. Then, SX test bars were solutionized and aged as standard heat treament process to obtain required structructure and high temperature mechanical properties. SX and heat treated parts were subjected to heat at two different high temperatures, 980ºC and 1100ºC, for two different long time, 1500 and 2000 hours, without applying any force under open atmosphere.

After structural examination, cubic γ' precipitates in AS-HT condition was observed to start to increase in size after holding for 1500 hours at 980ºC without any change in morphology but volume fraction of the particles began to dissolve in matrix phase. After 2000 hours, shape of the precipitates started lose their AS-HT morpohology and increase in size and decrease in volume fraction moved on. Following exposed to 1100ºC, dimensions of γ' phase were examined much higher than that of both AS-HT and 980ºC conditions. Also, morphology of the particles was completely change and broken for 1500 and 2000 hours. Precipitate amount was extremenly decreased according to AS-HT and holding at 980ºC.

In addition these structural changes, mechanical behaviour was examined via tensile testing at 982ºC after standard heat treatmen process and long term thermally exposure. It was resulted in higher elongation and tensile strength for AS-HT samples than samples held at high temperature for long time.

When fracture surfaces of both samples were examined, it was determined that both samples had typical ductile fracture behaviour due to dull and rough surface, and dimples in the structure.

# YÜKSEK SICAKLIĞA UZUN SÜRELİ MARUZ BIRAKILAN TEK KRİSTAL CMSX-4 SLS SÜPERALAŞIMIN YAPISAL VE MEKANİK ÖZELLİKLERİNİN İNCELENMESİ

## ÖZET

Nikel bazlı süperalaşımlar, yüksek sıcaklıklarda yüksek derecede kararlı olmalarına ve mekanik özelliklerine bağlı olarak havacılık sanayinde kullanılan gas türbin motorlarında en çok tercih edilen malzemelerdir. Uçak motorlarında 20.000-50.000 saat ve endüstriyel gaz türbinlerinde 100.000 saat yüksek performans gösterirken, günümüzde hareketli veya sabit gaz türbinlerinde kullanılan nikel esaslı süperalaşımlar, 1200°C'ye kadar yüksek oksidasyon direncine sahiptir. Bu alaşımlar, çok fazla sayıda alaşım elementi içermekte olup genellikle Periyodik Tabloda B grubunda yer alan elementlerden oluşmaktadırlar.

Nikel esaslı süperalaşımlar, 1940'lı yıllarda yaşanan II. Dünya Savaşı'nda gelişen uçak teknolojisiyle beraber ilk defa kullanılmaya başlanmıştır. Bu dönemde kullanılan ilk süperalaşımlar dövme yöntemiyle üretilmekte ve nispeten yüksek sıcaklıklarda kullanılmaktaydı. Uçak motor teknolojilerinin gün geçtikçe ilerlemesinin ardından motor giriş sıcaklıkları ve gereksinimlerindeki artışla beraber 1980'li yıllardan itibaren tek kristal nikes esaslı süperlaşımların ve üretim yöntemlerinin geliştirilmesine neden olmuştur. Tek Kristal nikel esaslı süperalaşımlar ise, genellikle gaz türbin motorlarındaki türbin bıçaklarının üretiminde kullanılmaktadır. Vakum altında kontrollü katılaşma ve yaşlandırma ısıl işlemlerinden oluşan özel döküm yöntemleri ve teknolojileri kullanılarak üretilmektedir. Tek Kristal üretiminde, Hassas Döküm yöntemi kullanılarak seramik kalıp üretimi gerçekleştirilir. İlk olarak üretilmek istene parçanın şekli mum enjeksiyon ile elde edilir. Yolluk, besleyici gibi yardımcı elemanlarla beraber döküm döküm modeli oluşturularak seramik kabuk üretimine başlanır. Bu döküm modeli, seramik çamurlara daldırılarak seramik kabuki üretimi tamamlanır. Bu seramik çamurlar kullanılacak alaşıma bağlı olarak alümina ($Al_2O_3$), zirkonyum silikat ($Zr_2SiO_4$) gibi farklı malzemeler olabilir. İçerisindeki mum, otoklav yönetimiyle boşaltılan ve pişirilen bu kalıplar daha sonrasında Vakum İndüksiyon Ergitme (VIM) ocağında döküm işlemine geçilir. Kalıp, vakum altında döküm sıcaklığına kadar ısıtıldıktan sonra eriyik metal kalıbın içeresine dökülür. Döküm gerçekleştikten sonra ergiyik metal, içerisinden soğutma suyu geçen bir bakıp plaka ve asansör sistemi aracılığıyla belirli bir yönde kontrollü olarak katılaştırılmaya başlanır. Bu yönlendirilmiş katılaştırma esnasında tane seçici adı verilen özel bir parça yardımı ile <001> yönünde katılaşmakta olan tanelerden bir tanesi seçilerek tek kristal üretimi tamamlanır. Soğuduktan sonra bu parçalar döküm modelinden ayrılarak yüksek sıcaklık mukavemeti kazandıran yaşlandırma ısıl işlemine tabi tutalarak kullanıma hazır hale getirilir. Uygulanan bu ısıl işlem, çözeltiye alma ve iki aşamalı yaşlandırma işlemlerinden oluşmakta ve bir kaç gün boyunca sürmektedir.

Tek kristal süperalaşım çeşitlerinden en yaygın olarak kullanılan ise 1980'li yılların sonuna doğru geliştirilen 2. nesil tek kristal alaşımı CMSX-4 alaşımıdır. CMSX-4

alaşımı, ağırlıkça %6,5 Cr, %9 Co, %0,6 Mo, %6 W, %6,5 Ta, %5,6 Al, %1,0 Ti, %3 Re ve %0,1 Hf elementlerinden oluşmaktadır. Özkütlesi ise 8,7 g/cm$^3$ olan bu alaşımın ergime sıcaklığı ise 1310ºC ile 1380ºC sıcakları arasındadır. İlerleyen zamanalar da ise bu alaşımı geliştiricisi ve üreticisi tarafında, yüksek sıcaklık mekanik özelliklerini ve oksitlenme direnci artırmak amacıyla CMSX-4 SLS alaşımı geliştirmiştir. CMSX-4 alaşımından farklı olarak içerisinde mekanik özellikleri iyileştirilmesi için daha düşük S elementi, oksitlenme direnci sağlayan La ve Y elementlerini içermektedir.

Bu yüksek lisans tezi kapsamında asıl amaç, tek kristal nikel esaslı süperalaşımlardan bir tanesi olan CMSX-4 SLS alaşımının yüksek sıcaklıklardaki davranışlarının incelenmesi ve anlaşılmasıdır. Bu amaç doğrultusunda test çubukları, ilk aşamada Hassas Döküm yöntemi kullanılarak <001> yönünde, vakum altında kontrollü bir şekilde katılaştırılarak tek kristal formunda üretilmiştir. Burada Tek Kristal, tane sınırlarının olmadığı bir iç yapı anlamına gelmektedir. Bu formun asıl amacı, yüksek sıcaklıklarda sabit kuvvet altında parçaların maruz kaldığı sürünmeye karşı mukavemetin artırılmasıdır. Tane sınırlarının iç yapıdan uzaklaştırılması ile sürünmenin en etkin mekanizmalarından biri olan tane sınırı kaymasının önüne geçilerek sürünme dayanamını artırılmaktadır. Tek kristal olarak üretilen bu parçalar, daha sonra çözeltiye alma ve yaşlandırma aşamlarını kapsayan yine vakum altında ısıl işleme tabi tutularak γ' parçacıklarının γ ana fazının içerisinde çökeltilmesi sağlanır. Yüksek sıcaklıktaki sürünme dayanımı etikeleyen bir diğer faktörler ise çökelen bu γ' parçacıklarının boyutu, şekli ve ana faz içerisindeki hacimsel oranıdır. Önceden yapılan çalışmalara göre bu fazların şekli kübik ve iç yapı içerisindeki oranı en az %70 olmalıdır.

Çökelti γ' fazlarının etkilerinin incelenmesi amacıyla tek kristal yapıya sahip ve ısıl işlemli test çubukları, yüksek sıcaklıktaki mikroyapısal ve mekaniksel özelliklerinin incelenebilmesi için herhangi bir yük kullanılmadan atmosfere açık ortamda iki farklı yüksek sıcaklığa iki farklı süre boyunca maruz bırakılmıştır. Bu sıcaklıklar 980ºC ve 1100ºC, süreler ise 1500 ve 2000 saat şeklinde uygulanmıştır.

Uzun süreli yüksek sıcaklılarda tutulduktan sonra çubukların, ilk olarak optik mikroskop ve Taramalı Elektron Mikroskobu (SEM) altında mikroyapısal özellikleri incelenmiştir. Bu incelemer sonucunda, standard ısıl işlem sonrasında tespit edilen kübik şekle sahip γ' çökeltilerin, 980ºC sıcaklığa 1500 saat boyunca maruz bırakılmasının ardından şekillerinin herhangi bir değişikliğe uğramadan boyutlarının artmaya başladığı gözlemlenmiştir. Aynı sıcaklıkta 2000 saat sonra ise, kübik şekillerinin bozulmaya başlamasının yanı sıra boyutlarındaki artışın devam ettiği tespit edilmiştir. Bu değişikliklere ek olarak hem 1500 saat hem de 2000 saat sonra, γ anafazı içerisindeki γ' parçacıklarının standart ısıl işlemli numuneye göre hacimsel oranının azaldığı görülmüştür. X-ray difraksiyon (XRD) ile gerçekleştirilen faz analizleri sonucunda ise ısıl işlemli numune de tespit edilen baskın γ ve γ' fazlarının, 980ºC sıcaklığa 1500 ve 2000 saat maruz bırakıldıktan sonra da baskın fazlar olduğu doğrulanmıştır.

Ayrıca genellikle servis koşullarında yani yüksek sıcaklık ve yük altında oluşan, mekanik özellikleri olumsuz yönde etileyen Topolojik Sıkı Paket (TCP) fazlarının oluşumu gözlemlenmiştir. Her iki süre sonunda 980ºC sıcaklıkta oluşan bu fazların SEM-EDS analizi ile benzer kompozisyonlara sahip olduğu belirlenmiştir. Bu fazlar, hacimsel olarak az miktarlarda oldukları için XRD analizinde bu fazlara ait herhangi bir sonuç elde edilememiştir.

Sıcaklığın 1100ºC'ye artırılmasıyla beraber hem 1500 hem de 2000 saat sonunda, γ' fazlarının kübik yapıları tamamen bozulma meydana gelmiştir. Boyutlarında ise ısıl işlemli ve 980ºC tutulan numunelere göre ciddi miktarda artış olduğu gözlemlenmiştir. Diğer yandan γ' çökeltilerinin iç yapı içerisindeki oranları ise 980ºC sonrası gerçekleşen azalmaya göre daha yüksek oranda azalmıştır. Bu durum γ' parçacıklarının, γ ana fazı içerisinde 980ºC sıcaklığa göre daha fazla çözündüğünü göstermektedir.

1100ºC sıcaklığa maruz bırakılan numunelerin iç yapısında 980ºC olduğu gibi TCP fazları olduğu görülmüştür. Fakat oluşan bu fazların, 980ºC oluşan TCP fazlarına göre SEM-EDS analizi ile farklı elementler içerdiği tespit edilmiştir. Analiz sonucu doğrutulsunda, iki farklı sıcaklıklarda oluşan TCP fazlarının farklı fazlar olduğu düşünülmektedir. XRD analizi sonucunda ise 980ºC tutulan parçalarda olduğu gibi hacimsel olarak az oranda oldukları için bu fazlara ait herhangi bir işaret gözlemlenmemiştir.

Yüksek sıcaklıktaki mekanik özelliklerin belirlenebilmesi için hem standard ısıl işlemli hem de uzun süreli 980ºC ve 1100ºC sıcaklıklara maruz bırakılan test çubukları ASTM-E8 standardına göre hazırlanarak ASTM-E21 standardına uygun olarak 982ºC sıcaklıkta çekme testi yapılmıştır. Yüksek sıcaklıkta gerçekleştirilen çekme testi sonuçlarına göre standart ısıl işlemli numunenin, uzun süreli sıcaklığa maruz bırakılan parçalara göre en yüksek mukavemete, 830 MPa, ve uzama oranına, %34, sahip olduğu görülmüştür. Standard ısıl işlemli numune 1500 ve 2000 saat boyunca 980ºC sıcaklıkta tutuldukta sonra mukavemetin 780 MPa değerine, uzamanın ise %20 oranına düşmüştür.

1100ºC sıcaklıkta 1500 ve 2000 saat bırakılan numunelerin mukavemetlerinde ise 710 MPa'a kadar düştüğü fakat uzamanın %20 civarında değişmediği gözlemlenmiştir. Çekme mukavemeti ve uzama oranlarındaki bu azalmaların nedeninin, standart ısıl işlemli numunenin iç yapısında bulunan kübik γ' çökeltilerinin sıcaklık ve sürenin etkisiyle kübik şekillerini kaybetmesi ve boyutlarının artması olarak düşünülmektedir.

Çekme mukavemetinde ve uzama oranındaki bu değişikliklerin yanı sıra, standart ısıl işlemli ve uzun süreli sıcaklığa maruz bırakılan parçaların elastic modüllerinde ve kesit daralmalarında herhangi bir artış veya azalış gerçekleşmemiştir. Ayrıca, sıcaklığın etkisiyle numunelerin iç yapısında bulunan zararlı TCP fazlarının mekanik özelliklere etkisi olup olmadığı bu fazlarının oranının çok düşük olması sebebiyle tespit edilememiştir.

Çekme testi sonrası kırılma yüzeyleri, dijital mikroskop makro ölçekte ve Taramalı Elektron Mikroskobu ise mikro ölçekte incelenmiştir. Bu incelemeler sonucunda makro ölçekte, kırılma yüzeyinin altında çeşitli boylarda çatlaklar oluştuğu gözlemlenmiştir. Kırılma yüzeyi incelendiğinde ise, kırılma yüzeylerinin mat ve pürüzlü bir yüzeye sahip olduğu görülmüştür. Kırılma davranışının net olaak anlaşabilmesi için Taramalı Elektron Mikroskobu ile analiz ediliğinde ise kırılma yüzeyinde kırılma gamzeleri olduğu tespit edilmiştir. Numuneler tane sınırına sahip olmayan tek kristal bir yapıya sahip olduğu için bu gamzeler, tane sınırları yerine γ' çökeltileri ve γ anafazı ara yüzeyinde oluştuğu tespit edilmiştir. Numunelerin kırılma yüzeylerinin, hem mat ve pürüzlü olması hem de kırılma gamze yapılarını içermesi nedeniyle tipik sünek kırılma davranışı sergiledikleri sonucuna varılmıştır.

# 1. INTRODUCTION

## 1.1 Purpose of Thesis

The aim of this study was investigation of effect of long term thermal exposure on microstructure and mechanical properties of CMSX-4 SLS single crystal nickel based superalloy and comparison with properties of CMSX-4 SLS single crystal superalloy produced in standard ways. While doing this, service condition was tried to imitate without applying any load by exposuring to heat for long time at high temperatures.

## 1.2 Nickel Based Superalloys

Nickel was discovered as a mineral (NiAs) by Swedish chemist Axel Fredrik Cronstedt in 1751 but it can be found in artificial goods produced in ancient times. For example, a zinc-nickel alloy known as white copper was used in China in 200 BC [1]. However, nickel alloys have started to develop in the beginning of 1900s with development of Gas Turbine Engines since new materials, that can stay stable at high temperatures and strees during operation of engines, were needed. Even though this increasing demand of high temperature materials, the term “superalloy” has been first used during World War II. [2], [3]

Superalloys generaly consist of Transition Metals like Fe, Ni, Co, W, Cr etc. in peridioic table [2] but there are three different types of superalloys according to base element; iron based, nickel based and cobalt based superalloys. The most popular and preffered kind of supperalloys is nickel based superalloys because the cost of nickel based superalloys is more affordable than cobalt based and the second reason is that they are more stable than iron based superalloys at elevated temperatures [4]. In addition to advantages, the key property of nickel based superalloys is FCC structure. This provides not only toughness and ductility but also stability from room temperatures to high temperature so nickel does not show phase tranformations up to melting point [4]. Therefore, they are preffered in high temperature applications such as turbine blades, disks, shafts, vanes in gas turbines and jet engines for aircrafts [5].

### 1.2.1 Single crystal nickel based superalloys

At beginning of application of nickel based superalloys, wrought products were preffered to produce turbine blades. However, turbine entry temperature, gas temperature that enters the turbine, is increasing with the improvements of new turbine engines as presented in Figure 1.1(a). And with developmet of vacuum induction casting technologies in 1950s, conventional cast alloys like MarM200, IN738LC etc. have been started to use in turbine blades [4]. When 1970 has come, Pratt & Whitney Aircraft has invented directional solidification (DS) technique which is used to produce oriented columnar grains in <001> direction to increase creep life high temperatures [6]. Advances in creep life time can be seen in Figure 1.1(b). In order to obtain best creep properties, first generation single crystal superalloys, which do not contain grain boundary strengthening elements C and B different from DS alloys, have been fabricated. In addition to removal of C and B, composition of precipitation hardening elements Al, Ti and Ta are increased [4]. With addition of 3 wt% Re to increase solid solution hardening and to prevent coarsening of γ’ phases, second generation superalloys like CMSX-4, PWA1484, has been developed. Also, it has lower Cr and higher Co content than first generation superalloy to minimize the formation of TCP phase. Third generation has appeared with increased Re content to about 6 wt% and reduced Cr content to 2,5 wt% but increased Re content caused increasing in tendency of TCP formation. At beginning of 2000s fourth generation superalloys, characterised by addition of Ru to improve stability of phases, took the scence. While both concentration of Re, Ru and Mo has increased in fifth generation alloys to develop temperature capabilities, sixth generation alloys has balanced amount of Cr, Re, Ru and Mo to enhance oxidation resistance [4], [7]. Compositions of both wrought and cast nickel based superalloys can be found in Appendix A in details.

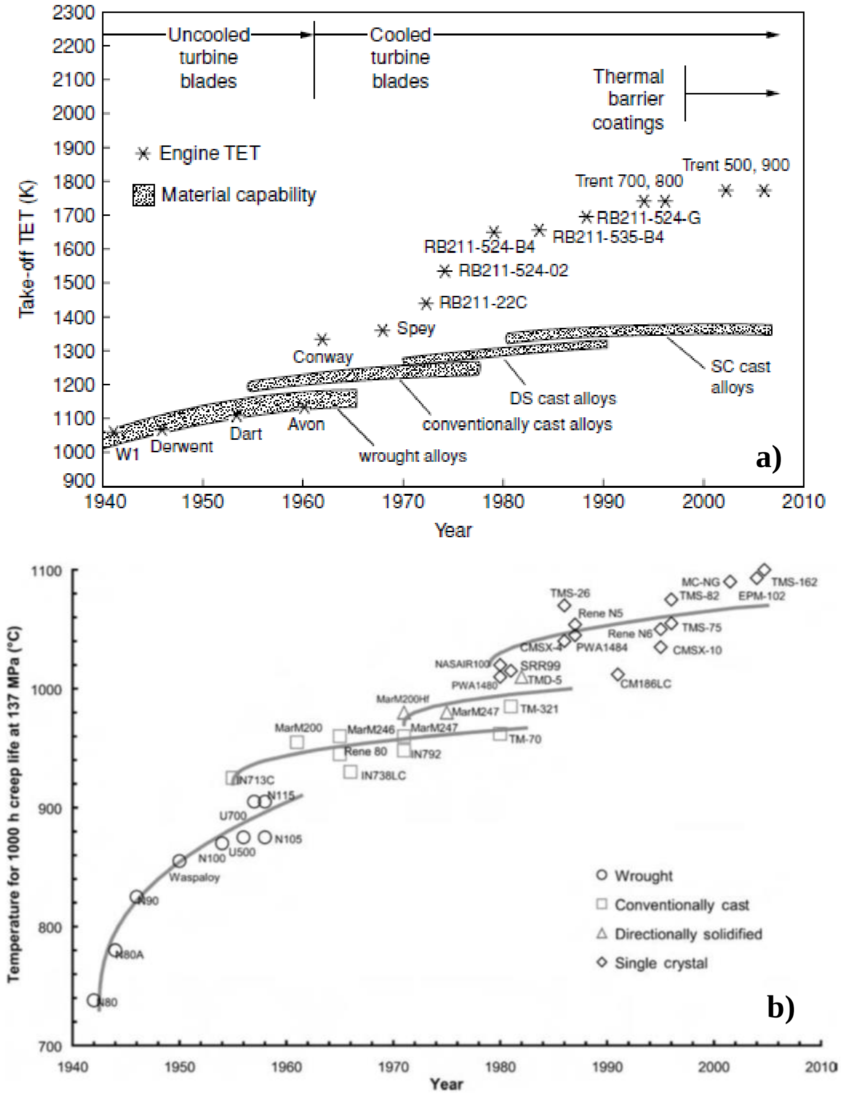

**Figure 1.1 : (a)** Turbine enrty temperature development from 1940 to 2010 **(b)** creep life time for various nickel based superalloys [4, 6]**.**

### 1.2.2 Microstructure of single crystal nickel based superalloys

Single crystal nickel based superalloys includes typically two main phases: relatively soft γ matrix phase and coherent strengthener γ’ phases. Since most of the single crystal nickel based superalloys have no carbon and/or boron (see Appendix A), carbides and borides, which can be found in many superalloys, did not discuss in details in this study but properties of all phases in nickel based superalloys were given in Appendix B.

#### 1.2.2.1 Gamma (γ) phase

Gamma (γ) is the matrix phase, which has Face Centered Cubic (FCC) structure, in all nickel based superalloys including single crystal superalloys and it generally consists of solid solution elements like Co, Cr, Mo, W, Re, and Ru [4, 5]. Gamma is relatively softer than the other phases [7]. And as shown in the Figure 1.2.a lighter regions represent γ phases in SEM image of the typical microstructure of a heat treated Ni-based superalloys.

Gamma phase also provides some advantages due to FCC structure. First one is that FCC structure has a high elactic modulus and multiple slip systems so mechanical properties like tensile, creep etc. are better than BCC and HCP structures [8]. Due to high atomic packing factor of FCC, alloying elements has lower diffusivity and mobility in FCC structure at high temperatures[8, 9]. And the last advantage is that FCC is very convenient to solid solution of alloying elements which can be used to precipitate intermetallic compounds like γ’ and γ’’ to increase strength at high temperatures.[8]

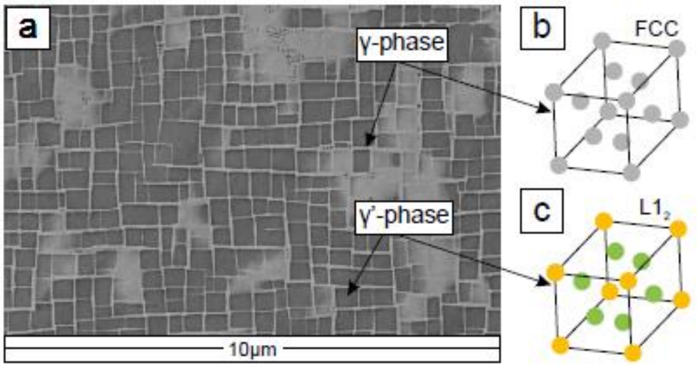

**Figure 1.2 : (a)** SEM image of the typical microstructure of a heat treated nickel based superalloy**,** schematic of **(b)** FCC and **(c)** $L1_2$ crystal structures [7]**.**

### 1.2.2.2 Gamma prime (γ’) phase

Gamma prime (γ’) is the main precipitation phase with $L1_2$ lattice structure coherent with γ matrix. Structure contains eight Al atoms at corners and eight Ni atom at the centers of faces as shown in Figure 1.2.c [4, 7]. It contains not only Al and Ti but also sometimes Nb, Ta and Cr and appears in sphere or cuboidal form (Figure 1.2.a) depends of the lattice mismatch between γ and γ’[5]. When it is rich in Nb, it can be denoted by γ’’ that is generally seen in nickel-iron superalloys instead of single crystal alloys [4].

Precipitation of γ’ phase is provide high mechanical strength at high temperatures which means that γ’ phase can act as a strong barrier against creep mechanisms, especially dislocation motion. The main reason behind this improvement is the lattice mistmatch between γ and γ’ which effects on the shape of γ’ precipitates. When it is in range of 0 and 0,2 percent, γ’ precitates become spherical shape. While increasing magnitude of mismatch between 0,5 and 1,0 percent causes cuboidal shape γ’ precitates, plate-like shape is produced above 1,25 percent of lattice mismatch [2, 5]. γ /γ’ interfaces become stronger with increasing lattice mismatch so dislocation movement hinders due to pile-up mechanism at the interface.

Another important factor affecting the high temperature strength is the size of γ’ phases. Strength increases with increasing particle size of precipitates until they reach the critical particle size [2]. Cutting mode for dislocation movement is dominant until the critical particle size but beyond this size bypassing mode becomes dominant. Therefore, this changing of dislocation movement causes a loss hardness and strength as shown in Figure 1.3. [2, 5]

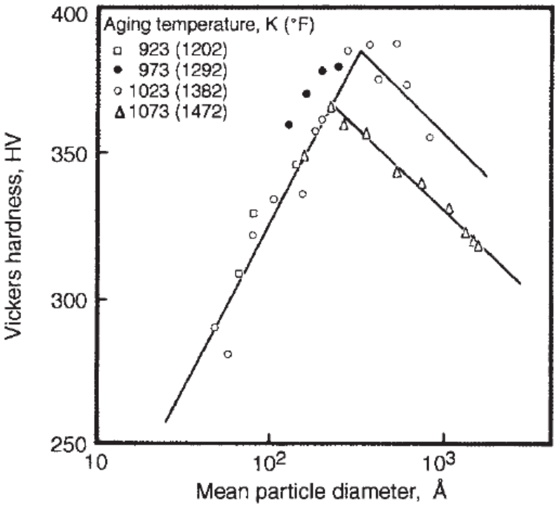

**Figure 1.3 :** Hardness versus particle diameter γ’ precipitates [5].

Altghough one of the most important features of γ’ precipitates is increasing yield strength with increasing temperature up to 800ºC, service temperature and life depend highly on coarsening of rafting and dissolution of γ’ phases [2]. The reason of this coherency between γ matrix and γ’ precipitates is lost by increasing lattice misfit due to rafting of γ’ particles [4].

Cubodial γ’ precipitates link up to to form plate or rod like morphology called as rafting of γ’ under an applied stress at elevated temperature during service [5]. Rafting morpohology depends on crystal orientation, lattice mismatch, load type and elastic modulus [2, 5]. Most SX alloys are oriented in <001> direction which results that rafted γ’ plates form perpendicular to tensile axis (Figure 1.4) causes negative misfit like in CSMX-4 alloy. If compressive stress is applied that mean positive misfit, needle like rafts develop parallel to loading direction [4, 5]. This $\gamma'$ lamellae are harmful for mechanical properties because of coarsening of $\gamma/\gamma'$ microsturucture [2]. During rafting, $\gamma$ partitioning elements like Cr, Re, W and Co diffuses out of $\gamma$ phase while $\gamma'$ partitioning elements like Al, Ti and Ta goes into $\gamma$. [4]

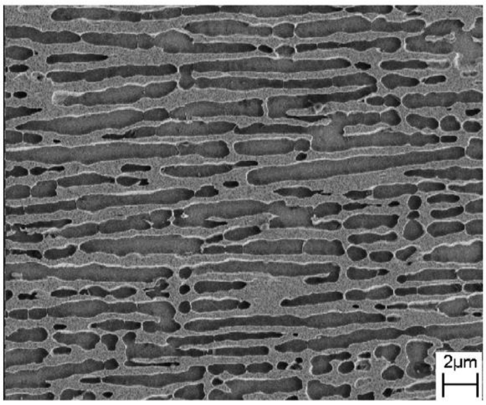

s

**Figure 1.4 :** Rafted $\gamma'$ phases in CMSX-4 alloy [10]**.**

#### 1.2.2.3 Topologically closed-packed (TCP) phases

Topologically closed-packed (TCP) phases are most detrimental phases among the phases in nickel based superalloys since they also form during service conditions, under load at high temperatures. They have generally needle- or plate-like shape so after formation, TCP phases act as stress concentration points, and they causes internal cracks and decreasing mechanical properties, especially creep strength and ductility, and failure [2, 5].

Transition metals like Co, Cr, W, Mo and Re are the main component of TCP phases beside nickel. Small changes in amount of Cr, W or Re determine which TCP phase becomes dominant and forms in the structure at certain temperature [11]. And general chemical formula is $A_xB_y$; A represents the group VIIB column including Mn and Re and B represents the other transition columns [12]. Therefore, when TCP phases start to nucleation and growth, amount of refractory elements in $\gamma$ matrix phase will decrease and effects of solid solution strengthening is reduced [7].

Four different types of TCP called $\sigma$, $\mu$, P and R as can be found in single crystal superalloys and summary of crystallographic informations and possible chemical formulas of 4 different TCP phases is given in Table 1.1.

**Table 1.1 :** Crystal structure of TCP phases [5, 7, 13]

| Phase | Crystal Structure | Space Group | Lattice Parameter (nm) | Chemical Formula |
|---|---|---|---|---|
| σ | Tetragonal | $P4_2/mnm$ | $a_o = 0.880–0.910$<br>$c_o = 0.450–0.480$ | FeCr<br>FeCrMo<br>CrFeMoNi<br>CrCo<br>CrNiMo<br>$Cr_2Re_3$ |
| μ | Rhombohedral | R3m | $a_o = 0.475$<br>$c_o = 2.554$ | $Co_2W_6$<br>$(Fe, Co)_7(Mo, W)_6$<br>$W_6Co_7$ |
| P | Orthorhombic | Pnma | $a_0 = 1.72$<br>$b_0 = 0.48$<br>$c_0 = 0.91$ | $Cr_9Mo_{21}Ni_{20}$ |
| R | Rhombohedral | R3 | $a_0 = 1.09$<br>$c_0 = 1.93$ | $Cr_{18}Mo_{31}Co_{51}$<br>$Fe_{52}Mn_{16}Mo_{32}$ |

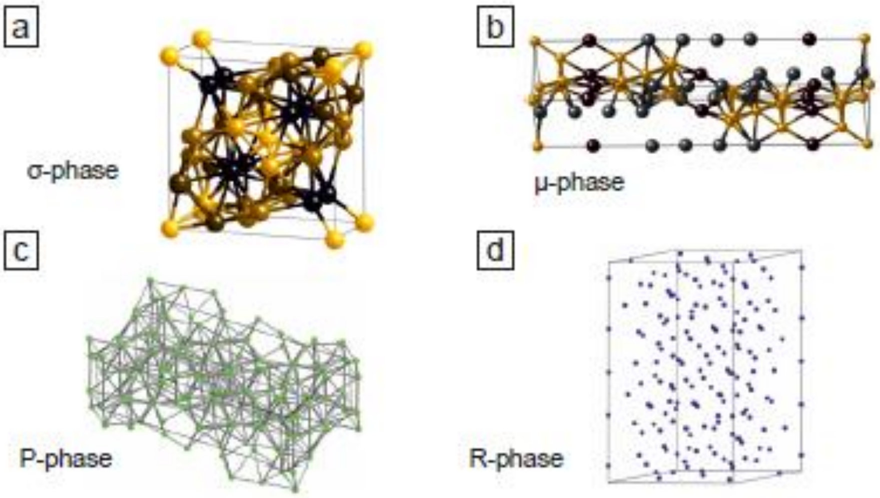

**Figure 1.5 :** Illustrations of structure of TCP phases: a) σ phase, b) μ phase, c) P phase and d) R phase [7].

*Sigma (σ) phase*

σ phase is a metastable TCP phase with tetragonal structure found in single crystal superalloys and start to forms as continues sheets at low temperatures below 950ºC in dendrite cores as shown in Figure 1.6 according to CALPHAD calculations stuied by Rae et.al [11]. When the temperature increases, σ phases become the nucleation sites for other TCP phases [13]. While it is rich in Ni and Cr, low amount of Mo and Re are included in σ phase [11]. Morpologhy of σ is generally feather-like as seen in Figure 1.7.a or plate-like and chemical formula is generally AB [13], [14].

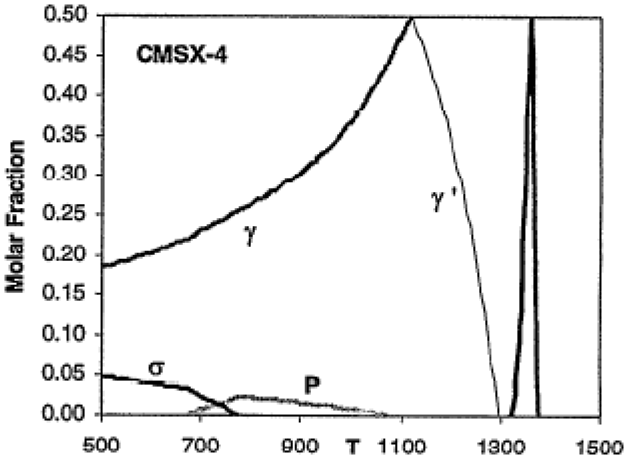

**Figure 1.6 :** Calculation of phase molar fractions in CMSX-4 single crystal superalloy [11].

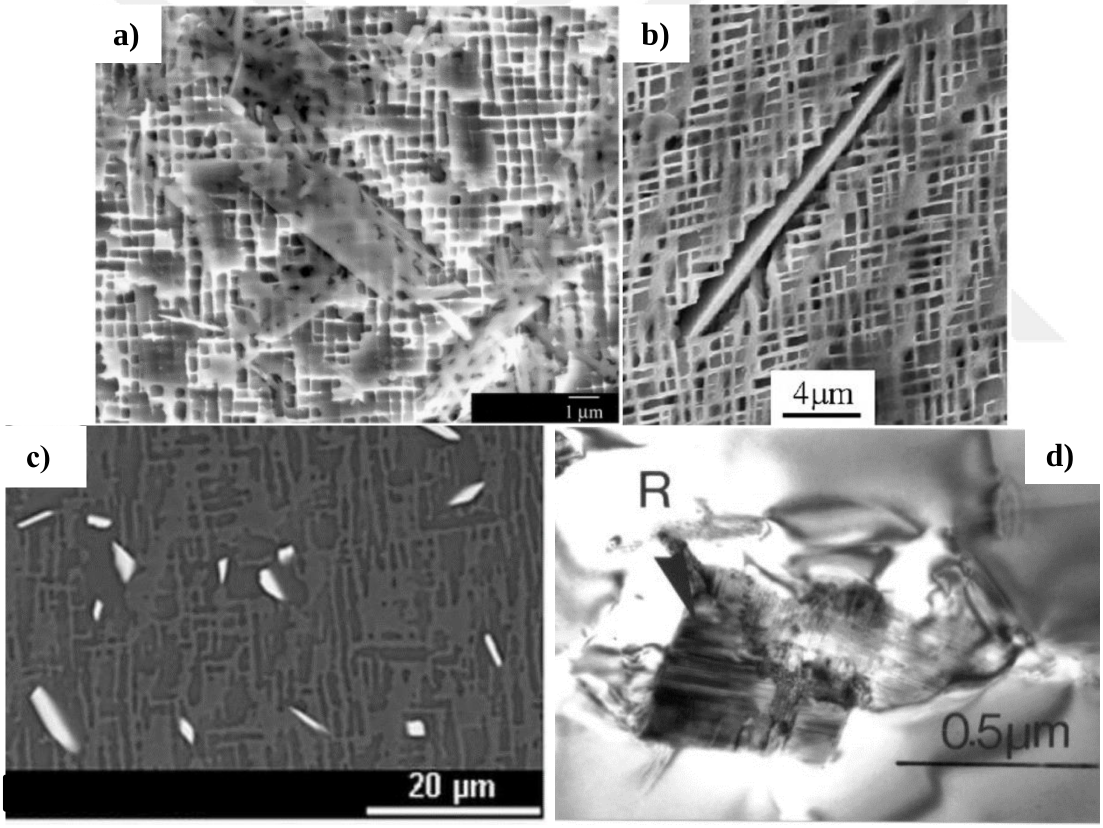

**Figure 1.7 :** SEM micrographs of **(a)** feather-like σ phase, **(b)** rod-like µ phase, **(c)** plate-like P phase and **(d)** R phase in single crystal superalloys [11, 13, 15].

*µ phase*

µ phase has chemical formula of $A_6B_7$ and rhombohedral structure. It appears as generally rod-like shape (Figure 1.5.b) but it can transform to need-like or blocky shape at different Re concentrations or high temperatures [13, 16], [17]. It stars to form at higher temperatures than 950ºC and while forming and growing, it consumes the σ phase [11]. It is mainly consist of Mo and/or W and lower Cr and Re unlike the σ phase, and also concentration of Co in μ phase is higher than in σ phase [11, 13].

*P phase*

Particles of P phase has plate-like shape as shown in Figure 1.5.c with primitive orthorhombic crystal structure. It generally forms in interdendritic regions which is poor in Re unlike σ and μ phase form in dendrite cores rich in Re [13] so Dubiel et.al found that P phase has richer in W content but lower amount of Re and Ni in CMSX-4 single crystal superalloy [18]. However, according to another research of Dubiel et.al while concentrations of W and Re are very high than other elements in both P and μ phases, P phase has higher percent of Cr and lower Ni and Co content than μ phase [19]. P phase is thermodynamically stable above 1100ºC and forms on metastable σ phase according to previous studies, and it can be found as only phase or also with μ and R phase [17].

*R phase*

R phase with rhombohedral cell is dominant in the interdentritic areas like P phase and has similar Cr and Mo composition to P phase [11], [13]. Morphology of R phase is irregular due to forming sporadically (Figure 1.5.d) [11].

### 1.2.3 Production of single crystal nickel based superalloys

Investment casting or lost-wax process is used to produce near-net shape products with high accuracy of surface smoothness, shape and dimesions [20]. And it gained an significant role in modern metal casting techniques with the increasing demand of near-net shape product. Invesment casting can be applicable in various industries such as automotive, marine, power plant, missiles but it had a key position in aviation industry since World War II especially in production of engine parts like, turbine planes, vanes, nozzles etc. due to their complex shapes. [20]

In Figure 1.8, steps of investment casting process are summarised. At beginning of the investment casting method, a metal injection tool or die is machined according to shape of product and then the wax is injected into the metal tool. After the injection, wax model of the part is assembled with auxiliary patterns, pouring cup, risers, sprue and so on to make complete casting model or called as tree for ceramic mold. Next, the casting model is dipping into ceramic slurry, that can be also called as investment, and coated with this slurry. The slurry is mixture of binding agents and ceramic powders like zircon ($ZrSiO_4$), alumina ($Al_2O_3$) and silica ($SiO_2$). After dipping, same ceramic powders used in slurry pour out slurry coated model and it is called as "stuccoing" and it is left for drying. These dipping, stuccoing and drying steps are repeated several times to reach requested shell thickness. When the adequate shell thickness is complete, the mold is ready to dewaxing operation under high pressure water vapour in a steam autoclave. After removing wax, firing or sintering is applied on green body in order to increase the strength. Finally, it is ready to casting under atmosphere or vacuum environment. [4, 5, 20]

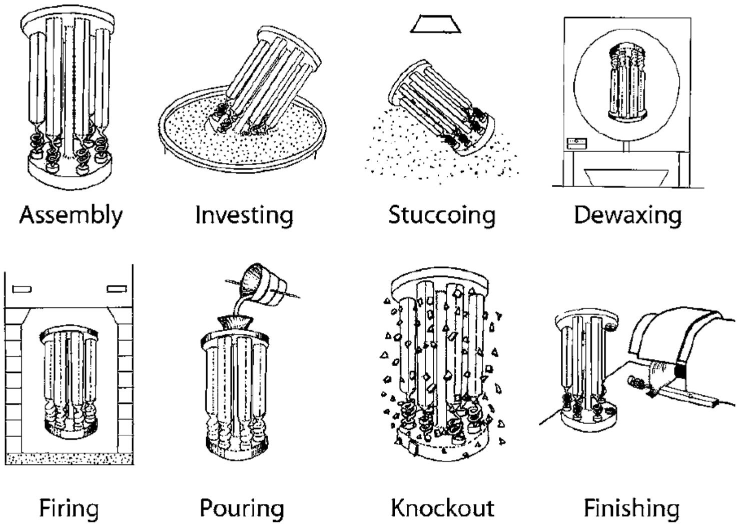

**Figure 1.8 :** Stages of investment casting process [4].

Nowadays the biggest market of investment casting is superalloy turbine blades since it can be used for production of polycrystalline parts, directionally solidified or columnar grain and single crystal products [4, 5]. After conventional mold preparation, the superalloys is melted and poured into mold in Vacuum Induction Melting (VIM) furnaces under vacuum since elements with high oxygen affinity like Al, Ti in superalloys can react with oxygen in atmosphere [21]. However, special furnaces and techniques are need for casting of single crystal superalloys rather than equiaxed grain casting. There are several methods to produced directional solidified single crystal superalloys but the most common one is Bridgman method also called as high-rate solidification method. Bridgeman type of VIM furnaces comprise of basically two chambers; melting or heating chamber and cooling or withdrawal chamber (Figure 1.9(a)). A radiation baffle is placed between these chambers to reduce heat loss and increase thermal gradient. After reaching suitable vacuum values, fired ceramic mold on cupper chill plate is raised into heating furnace with help of the lift and heated up to casting temperature. This temperature is generally above 1500 ºC for SX casting. During heating of ceramic mold, mother alloy ingot is started to melt and when it becomes completely liquid and reaches to pouring temperature, liquid metal is poured into mold. And then, lift moves down to cooling chamber with a set withdrawal rate which is typically in the range of 2-5 mm/min. Nucleated grains are aligned towards to <001> direction during withdrawing process. [21–23]

A grain selector in the form spiral shape or a seed should be used at bottom of the mold to remove grain boundaries and produce single crystal part. A grain selector consists of a starter block and a spiral also called as pig-tail. After pouring, solidification starts from to starter block and pig-tail allows only a single grain out of several alongated grains in <001> to pass into part cavity as shown in Figure 1.9(b) [21, 22]. Seed is the other method to produce SX structure. Seed can be in different crystal orientations, <110>, <111> etc. rather than <001> which is the main difference from the grain selector and advantage. Parts can be easily produced with specific crytal directions. [21, 23]

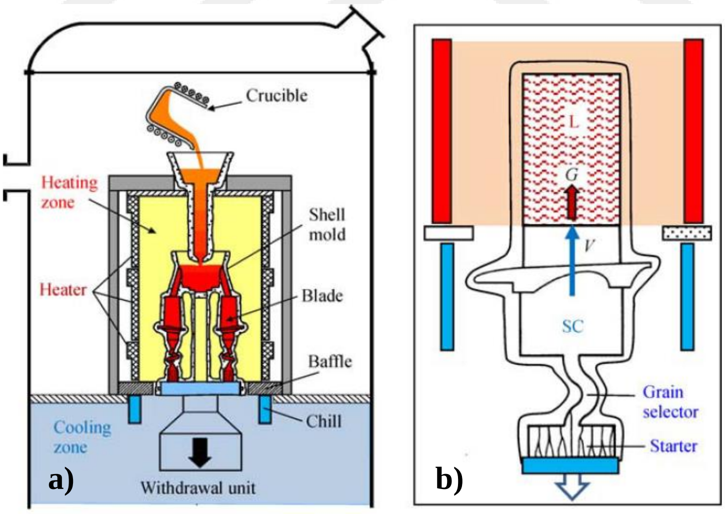

**Figure 1.9 : (a)** Schematic drawing of Bridgman furnace, **(b)** solidification with grain selector [22].

### 1.2.4 Heat treatment of single crystal nickel based superalloys

As-cast microstructure of CMSX-4 SX superalloys consists of two phases γ and γ’. The previous studies showed that during solidification Co, Cr, W and Re prefentially segregate to the dendrite cores unlike Ti, Al and Ta which diffuse to interdentritic regions [24]. And while γ phase is the primary phase in dendrite cores, γ- eutectic islands with coarse, irregular shaped and incoherent γ’ precipitates form at the final stages of solidification in interdendritic regions as presented in Figure 1.10 [21, 25, 26]. To solve this compositional segregation problem, first step of heat treatment of SX alloy must be homogenization practiced under vacuum to avoid oxidation [21, 26]. To dissolve these coarse γ’ precipitates, alloy must be heated above solvus temperature of γ’ for a few hours but the temperature should be below liquidus line [26]. Solutionizing temperature of CSMX-4 alloy is generally between 1277ºC and 1322ºC and it takes almost a full day [24, 27]. Then quenching is applied with argon gas circulated using fans to maximise cooling rate for preventing of coarsening of γ’ particles and to obtain homogeneous cooling in the furnace [21, 28]. Homogenised γ matrix and irregular γ’ precipitates with size of 0,3-0,5 μm appear after complete solution heat treatment [21, 25].

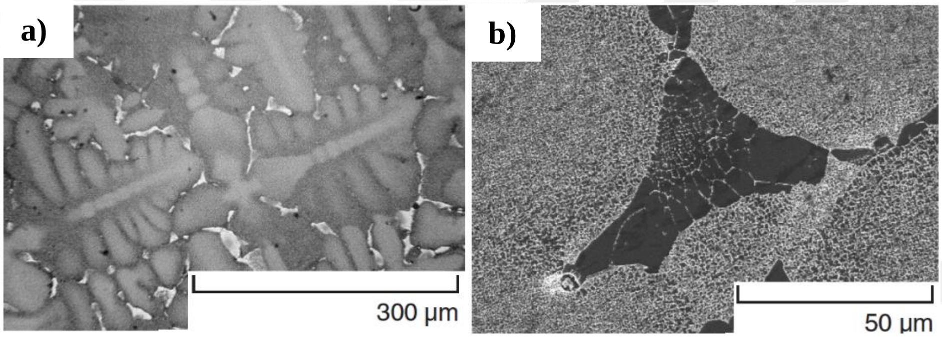

**Figure 1.10 :** **(a)** Dendritic structure occurs during solidification **(b)** γ’ island in interdendritic region [27].

Two steps aging heat treatment takes place following solution heat treatment. It is performed below the solvus temperature but for longer time than solutionizing [26]. For CMSX-4 alloy, primary aging is applied for 4 hours about 1080°C and secondary aging is practiced for 16 hours around 870°C [29]. The aim of the aging step is to adjust the morphology and size of γ’ phases to improve the mechanical properties especially at high temperatures [28, 30]. Ricks et al. showed that morphology of γ’ precipitates grows in order of spheres, cubes and arrays of cubes during aging treatment and cubes become larger with increasing degree of aging as shown in Figure 1.11.a [31]. Finally, γ’ precipitates has uniform cuboidal shape (Figure 1.11.b) and approximately 0,5 μm size. [25]

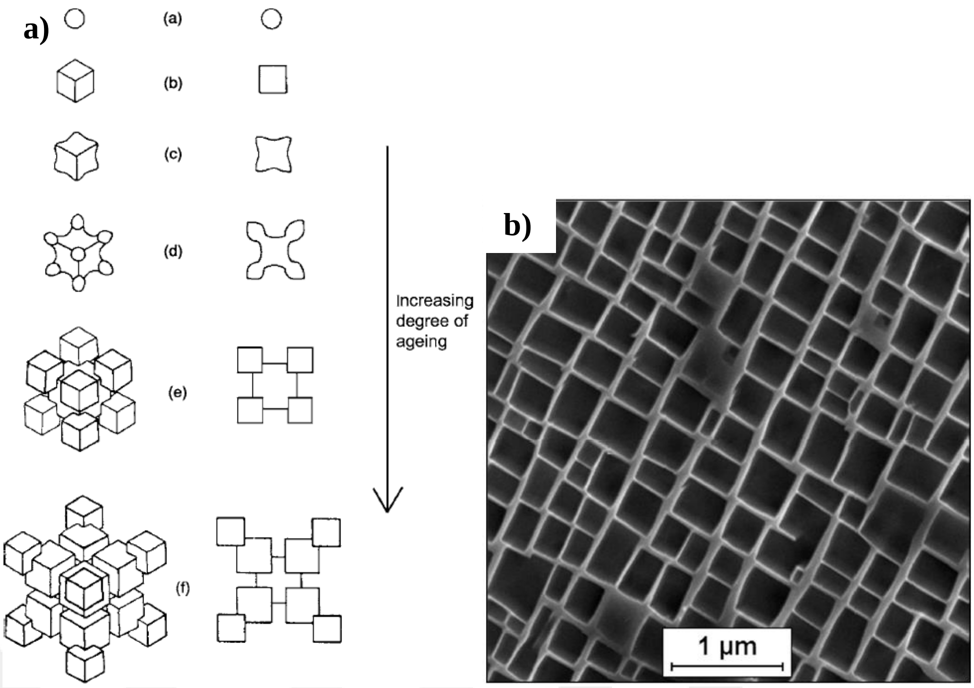

**Figure 1.11 : (a)** Illustration of γ’ precipitate development in <111> (left) and <001> (right) projection and **(b)** Cubic morphology of γ’precipitates (darker regions) and γ matrix (lighter regions) [25, 31].

### 1.2.5 Mechanical properties of single crystal nickel based superalloys

Mechanical properties of single crystal superalloys are quite critical for long life time of turbine engine blades.

Changes in yield strength of single crystal alloy CMSX-4 due to temperature is given in Figure 1.12. While the yield strength is aroun 800 MPa up to 700ºC, it increases to 900 MPa at 750ºC. However, when temperature becomes higher than 900ºC, yield strength falls to 600 MPa at 950ºC. And after reaching 1100ºC, yield decreases very rapidly 150 MPa [4]. So it can be said that the yield strength of superalloys increases with increasing temperature up to a peak temperature, after reaching this peak it falls very rapidly [4, 32]. To understand reason of this behaviour, different studies have been conducted. Lall et.al [33] has found that octahedral slip systems are more dominant at temperatures below peak temperature during loading whereas cubic slip systems dominates when temperature is above peak stress tempreature. Another study shows that dislocations expand on γ’ phase at lower temperatures and γ matrix controls the mechanical properties while γ matrix become host for dislocation expansion and mechanical properties become dependent on γ’ precipitates at higher temperatures [34].

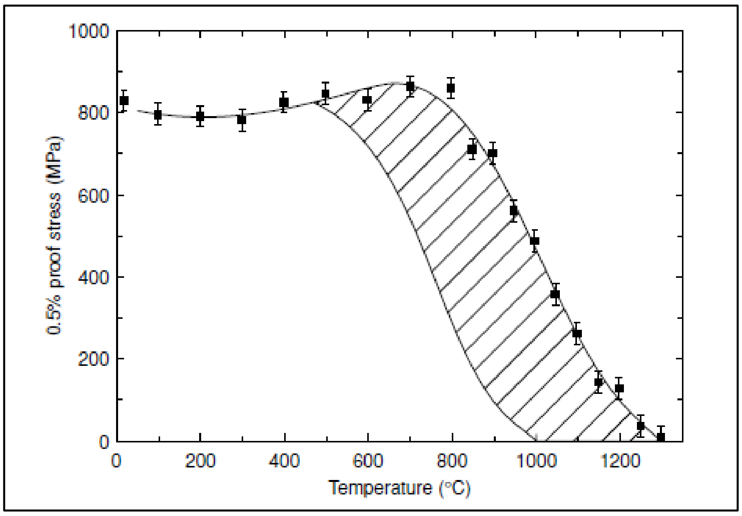

**Figure 1.12 :** Yielding behaviour of single crystal CMSX-4 orientated in <001> direction at different temperatures [4].

Creep mechanism in <001> oriented single crystal alloy is affected by not only temperature like yield stress but also stress as given in Figure 1.13. At low temperatures with high stress levels (Figure 1.13(a)), creep strain rate increases in the beginning and then decreases with increasing creep strain which is called as primary creep deformation. Then, secondary creep period, existing in all single crystal superalloys, follows and most of the creep life is in this period. When the creep deformation occurs at relatively intermediate conditions like 950ºC and 186 MPa (Figure 1.13(b)), tertiary creep deformation can be observed. During this stage, strain rate promotes monotonically with increasing creep strain. Unlike the polycrystalline alloys, single crystal alloys have no steady-state creep under constant strain rate. And creep curve appears as a plateau with reaching beyond 1050ºC as shown in Figure 1.13(c). After this plateau, creep strain increases very rapidly following immediate failure. The reason of this sudden failure is degradation of γ/γ’ microstructure called as rafted morphology or rafting regime.[4, 35, 36]

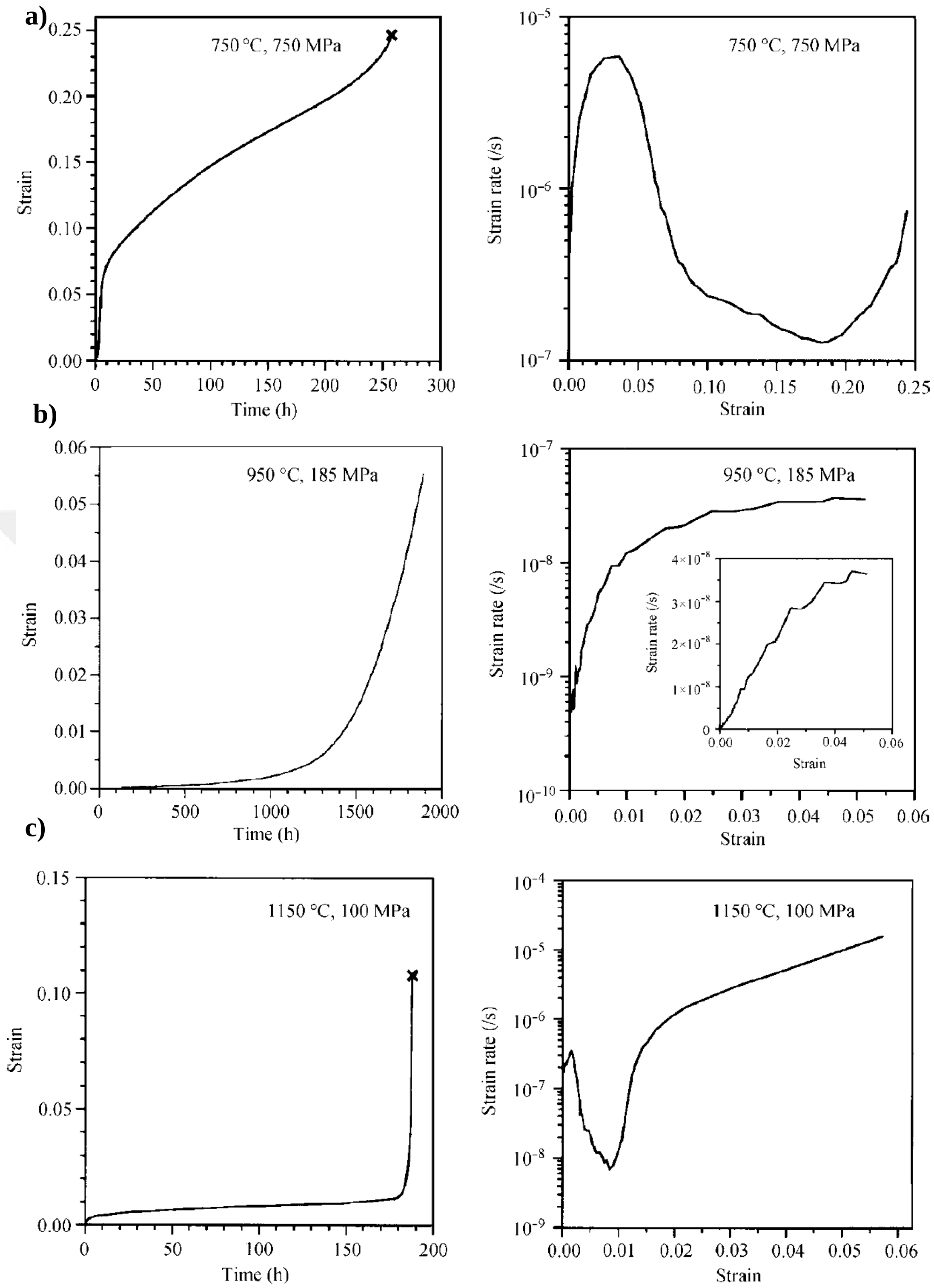

**Figure 1.13 :** Creep behaviour of single crystal CMSX-4 orientated in <001> direction at different temperatures and stresses [4, 35, 36].

# 2. MATERIALS & METHODS

## 2.1 Production of the Samples

Second generation single crystal nickel based superalloy CMSX-4 SLS was supplied from Cannon Muskegon (USA), manufacturer of the alloy, and composition of the alloy was given in Table 2.1. For investment casting, waxes were purchased from Remet UK Ltd. (England) and ceramic molding materials, zirconium silicate ($ZrSiO_4$) powders, fused alumina powders and binders, were supplied from England.

**Table 2.1 :** Chemical composition of CMSX-4 SLS nickel based superalloy in percentage.

| Cr | Co | W | Ta | Al | Ti | Mo | Re | Hf | La+Y | S | Ni |
|---|---|---|---|---|---|---|---|---|---|---|---|
| 6,5% | 9,0% | 6,0% | 6,5% | 5,6% | 1,0% | 0,6% | 3,0% | 0,1% | 0,002% | max 1,0 ppm | bal. |

First, eight cylindrical test bars with 13 mm diameter and a height of 200 mm were injected into Aluminum injection tool by using injection machine. To use in production of single crystal, wax injected pig tail was produced. After finishing injection steps, test bars were asssemled with pig tails and feeders to create a casting cluster as shown in Figure 2.1.a. Following the cluster assembly, for dipping of the cluster three differents zirconium silicate based slurry, which has different viscosity values, and for stuccoing fused alumina powders were used in each coats. The cluster were dipped into first and second slurries as primary coats and then for back up coats third slurry was used. And between in each dipping and stuccoing steps, the cluster was left min 4 hours for drying. Dewaxing was the following step. During dewaxing 8 bar pressure and 180ºC temperature were applied for 10 minutes. Then the green body was sintered in 800ºC for 1 hour.

Fired ceramic mold (Figure 2.1.b) was placed in ALD VIM-IC10 (Germany) furnace which is a Bridgman-type furnace. CMSX-4 SLS alloy was melted and poured into ceramic mold at 1560ºC under vacuum of $10^{-3}$ mbar. After pouring, the mold was withdrawn with rate of 4,3 mm/min in <001> direction for controlled directional solidification. When temperature of the mold became at room temperature, it was taken from VIM furnace and knocked-out to separate ceramic mold and solidified test bars. And picture one of the test bars was given Figure 2.1.c.

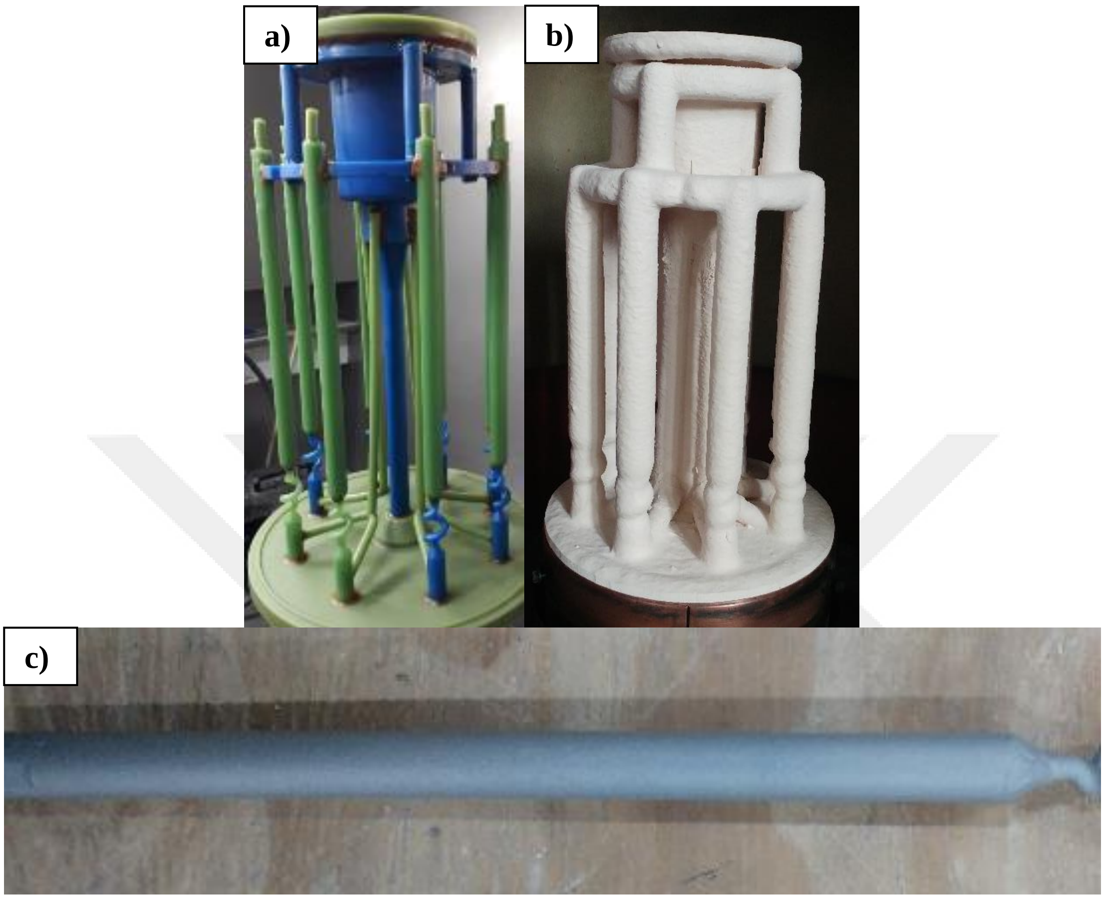

**Figure 2.1 : (a)** Cluster of test bars, **(b)** fired mold and **(c)** one of test bars after casting.

After knocking-out of ceramics solutionizing and aging heat treatments was applied in TAV Vacuum Heat Treatment (Italy) furnace to test bar in order to create cubic form of γ’ phase. As given Figure 2.2, first, test bars were held at 1320ºC for 18 hours to solve γ’ phase into matrix γ phase then quenching was applied by using Argon gas to decrease temperature from solutionizing temperature to room temperature. For primary aging, the temperature was increased to 1140ºC and held for 2 hours. After primary aging, secondary aging was applied at 871ºC for 20 hours as a final step of heat treatment.

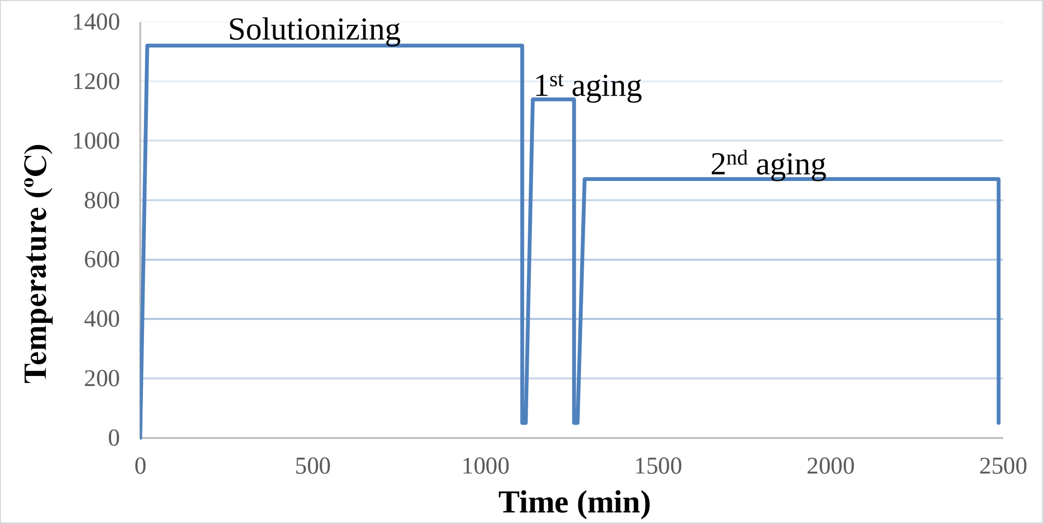

**Figure 2.2 :** Heat treatment cycle of CMSX-4 SLS single crystal alloy.

In order to check crystallinity of test bars, they were etched in macroscale by solution of 20% water, 20% hydrochloric acid (HCl) and 60% hydrogen peroxide ($H_2O_2$) supplied from local markets. Etched image of test bars were given in Appendix C.

After ensuring single crystal structure of test bars, misoriention α angles (Figure 2.3) in <001> direction were measured via back-reflection Laue XRD method according to standard of ASTM E82-91. Laue technique is used to determine quantitavely single crystal orientation by production of diffraction spots of the sample [37]. Laue is the simplest and easiest method to make diffraction pattern, and works with white radiation. It composes of a x-ray tube, specimen holder, collimator and cassette (Figure 2.4 (a)). Laue camera ans x-ray tube must be correctly oriented to create diffraction spot. After placing the specimen on the specimen holder, radiation from x-ray tube is reflected back from specimen. Then, it goes through collimator and is collected by cassette [38]. Therefore, Laue pattern (Figure 2.4 (b)) are created and ready to analyse.

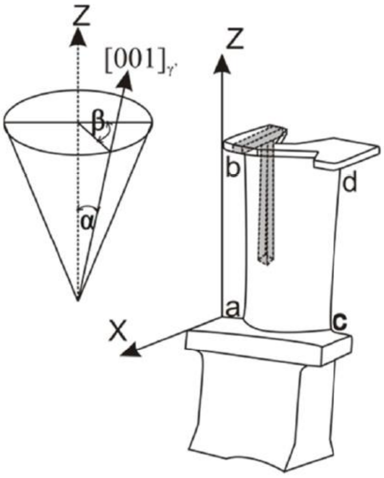

**Figure 2.3 :** Schematic drawing of misorientation α angle [39].

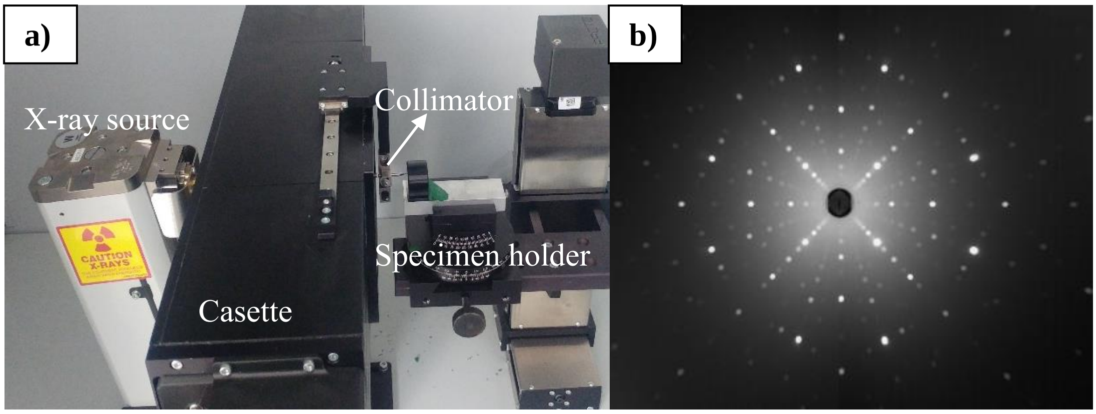

**Figure 2.4 : (a)** Instruments of Laue XRD and **(b)** an example of Laue pattern [40].

Deviation angle should be below 15º for single crystal superalloys but to reach maximum mechanical properties at high temperature, it should be less than 10º as found in previous studies [4, 35]. For examination of misorientation angle, Proto XRD Laue COS machine were used with Mo X-ray tube at room temperature, and 40 kV acceleration voltage and 30 mA tube current was applied during measurement. Misorientation angles and Laue patterns of the samples can be found in Table 2.2 and Appendix D. According to analysis results of all test bars had convenient misorientation angles for next steps of experimental procedures.

**Table 2.2 :** Misorientation angles of test bars after standard heat treatment.

| Test bar | No 1 | No 2 | No 3 | No 4 | No 5 | No 6 | No 7 | No 8 |
|---|---|---|---|---|---|---|---|---|
| **Misorientation angle, α (º)** | 6,27 ± 0,06 | 7,97 ± 0,68 | 8,83 ± 0,15 | 3,27 ± 0,45 | 6,50 ± 0,44 | 2,10 ± 0,56 | 8,90 ± 0,56 | 9,63 ± 0,58 |

## 2.2 Long Term Exposure of the Samples at Elevated Temperature

After application of standard heat treatment, eight test bars was subjected to two different temperature and holding time for investigation of changes in structure. 980°C and 1100°C was chosen as exposure temperature while exposure time was 1500 and 2000 hours. While four test bars were held at 980°C, other four test bars from same casted parts were exposed to 1100°C in different furnaces. After 1500 hours two test bars were taken out from the furnace at 980°C and two test bars from furnace at 1100°C, and waiting for cooling in air while the others were remained in furnaces at thesee temperatures. When 2000 hours were completed, remained test bars were pick from furnaces and left to air cooling. During long-term thermal exposure, no partial pressure was applied and both two furnaces were open to atmosphere.

## 2.3 Characterization Techniques and Equipments

### 2.3.1 Structural Examination

For structural examination, first samples cut from bottom of the each bars parallel to [001] plane (Figure 2.5) after both heat treatment and long time exposure processes. After conventional preparation for metallographical examination, samples were etched for a few seconds with same etchant, solution of water, hydrochloric acid (HCl) and hydrogen peroxide ($H_2O_2$). Olympus BX53M optical microscope at TUBITAK MRC and Philips XL 30 SFEG SEM at Gebze Technical University was used to investigate changes in microstructures of the samples. While doing this, sizes and percentages of γ’ precpitates were measured from different grains and regions, and shapes of γ’ phases were examined.

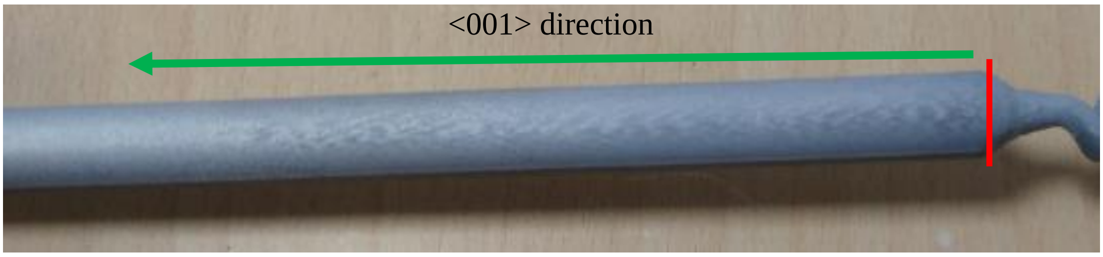

**Figure 2.5 :** Sampling of test bars.

Same as-heat treated and long time exposure samples was analysed by Rigaku Smartlab XRD machine between 20° and 120° with step degree of 0,020 to examine existed phases in the samples. XRD patters was examined by using High Score Plus software and intensity ratios of each peak were calculated by dividing strongest peak in the patterns of both AS-HT and long term exposure samples.

### 2.3.2 High Temperature Tensile Testing

Zwick/Roell Z600 tensile testing equipment in TUBITAK MRC was used to determine high temperature mechanical properties of as-heat treated and long time exposure samples. Tensile tests were applied under 400 pre-load of at 982ºC with 0,0014 $s^{-1}$ strain rate according to ASTM E21 standard. Two tensile test specimens were extracted from each test bars with 13 mm diameter and 180 mm length (figure) and prepared with 30,0 mm gauge length and 6,0 mm diameter according to ASTM E8 [41]. A green oxide scale (Figure 2.6) was observed on surface of each long time exposure test bars and to remove this oxide scale and to reach main structure of the SX alloy, these dimensions were chosen.

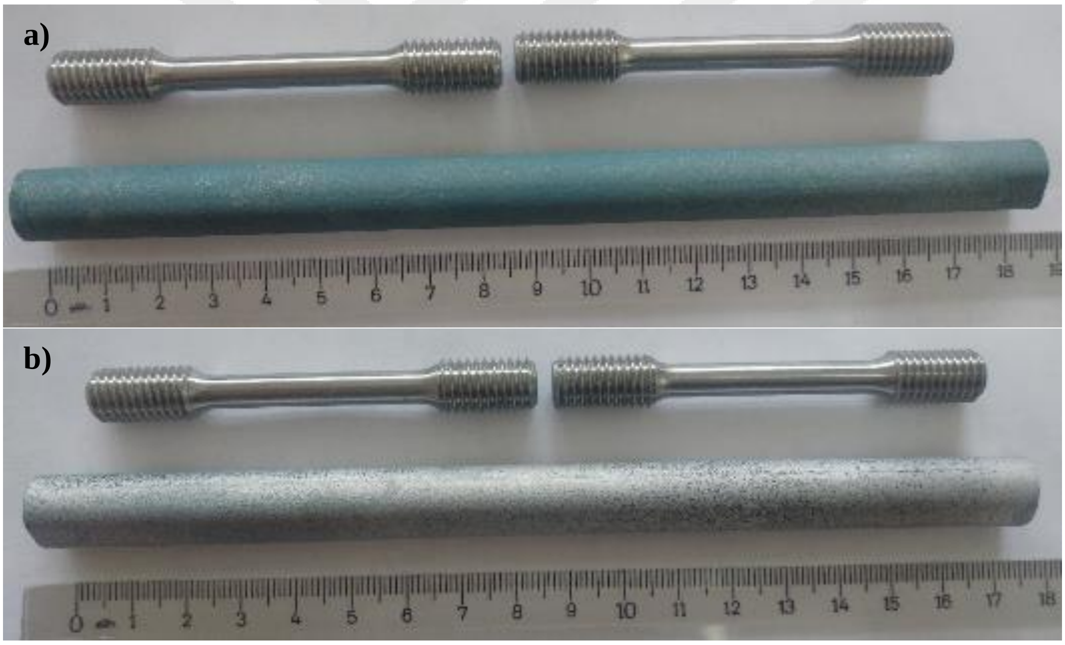

**Figure 2.6 : (a)** One of the test bars after held 980ºC for 1500 and 2000 hours, **(b)** One of the test bars after held 1100ºC for 1500 and 2000 hours.

Following the tensile testing, fracture surfaces of both specimens were examined under Hirox RH-2000 digital microscope and JEOL JXA-840A to observe effect of long term exposure on fracture mechanisms.

# 3. RESULTS AND DISCUSSION

## 3.1 Structural Futures of As-Heat Treated Samples

After standard heat treatment of CMSX-4 SX superalloy, cuboidal γ’ preciptates were obtained as seen in SEM micrographs in Figure 3.1(b). However, they can not be seen clearly under optical microscope since size of these phases were 0,38 μm (± 0,07) due to SEM photographs. Also, percentage of γ’ particles was measured as 74,19% (±1,69) so volume fraction γ matrix was 25,81% (±1,69) in the structure. Furhermore, there was no existence of any TCP phases. These results matches with previous studies done by Dubiel et.al [19] who found γ’ particles with fraction of 78% and size of 0,37 μm after similar heat treatment procedure. In another research, Murakumo et.al [42] have studied effect of γ’ volume fraction on mechanical behaviour of SX alloys and obtained maximum strentgth when the volume fraction was about 70%. Also, Reed [4] stated optimum fraction of the precipitates is approximately 70% to reach maximum strength at high temperatures.

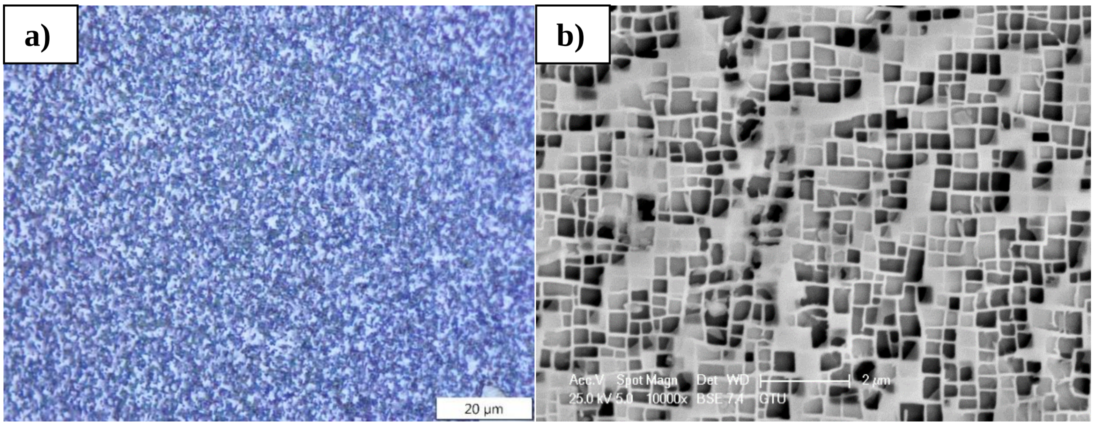

**Figure 3.1 : (a)** Optical microscope images under 150x magnification and **(b)** SEM images under 10000x magnification after standard heat treatment.

Although XRD pattern of AS-HT sample had one extremely strong at 50,88º, one relatively weak peak at 118,40º and smaller peaks at 24,80º, 45,60º, 80,20º and 101,78º as seen in Figure 3.2. And all included peaks and intensities ratios of these peaks were given in Table 3.1. Strongest peak was at 50,88º angle with intensity of 100 million counts which belongs to [200] plane of both γ and γ’ phases as expected due to solidification direction. Other smaller one indicated at 2θ of 118,40º belongs to [040] plane of both γ and γ' phases. These 2θ angles and patterns match with given patterns of γ and γ' phases in Figure 3.3 which shows that some planes of two phases are parallel to each other like <111>, <200> etc. so 2θ angles of these planes overlap each other at same angles [43]. And Bai [44] found the greatest peak for [200] plane at around 50º and smaller [010], [111] and [030] peaks at about 2θ angle of 25º, 44º and 80º for single crystal CMSX-4 superalloy in his study.

**Table 3.1 :** 2θ angles and intensity ratios in XRD patterns of AS-HT.

| **Phase** | 2θ angle (º) | Intensity ratio (%) |
|---|---|---|
| **γ' [010]** | 24,80 | 0,14 |
| **γ and γ' [111]** | 45,60 | 0,23 |
| **γ and γ' [200]** | 50,88 | 100,00 |
| **γ' [030]** | 80,20 | 0,07 |
| **γ' [032]** | 101,78 | 0,02 |
| **γ and γ' [040]** | 118,40 | 3,23 |

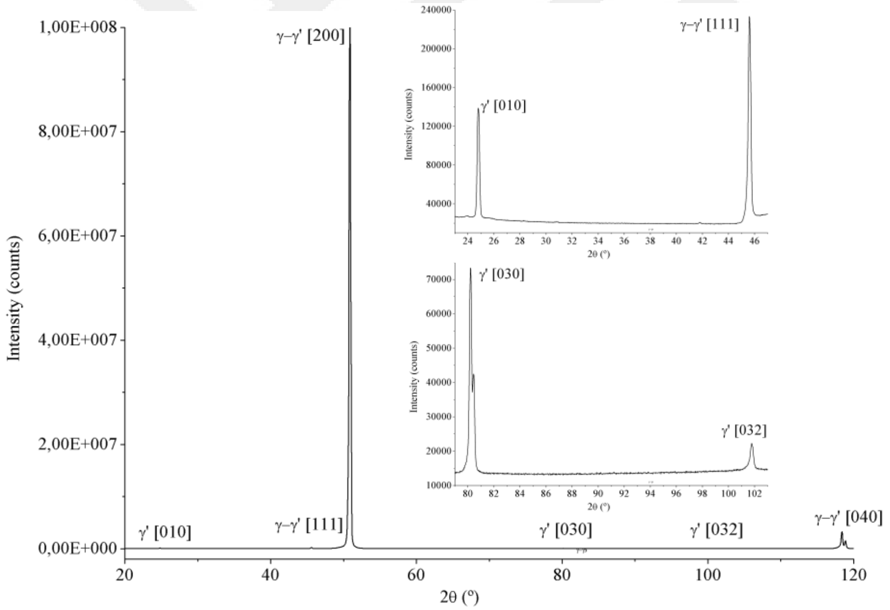

**Figure 3.2 :** XRD pattern of AS-HT sample.

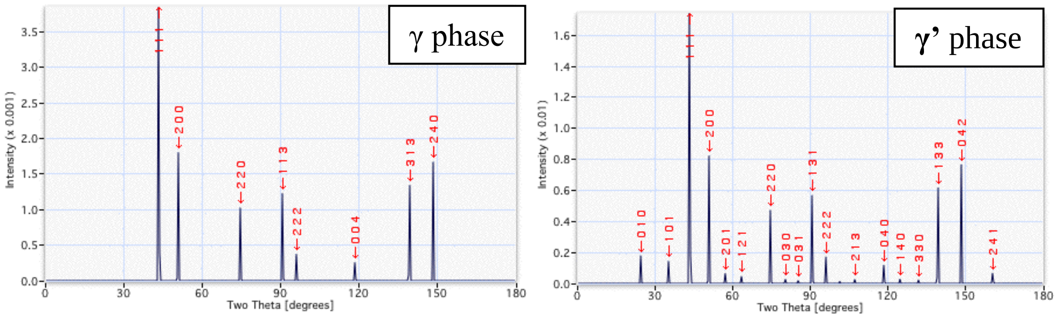

**Figure 3.3 :** Typical XRD patterns of γ and γ' phase [43].

## 3.2 Structural Futures of Samples Held at 980°C for 1500 and 2000 Hours

Changes in microstuructures of the samples held at 980°C for 1500 and 2000 hours have been observed and can be seen in Figure 3.4. After 1500 hours, γ’ precipitates started to grow from 0,38 μm (±0,07) to 0,73 μm (±0,39) while they preserved their cubic morphology as shown in SEM image in Figure 3.1.d but these change in size of precipitates could not be seen obviously in micrograph under optical microscope. When holding time increased to 2000 hours at 980°C, morphology of γ’ phases disintegrated from perfect cubic shape and coarsening of them observed still moving on (Figure 3.1.f). It grew up to 1,12 μm (±0,55) and they could be seen barely by optical microscope as shown in Figure 3.1.e. In addition to these changes, volume fraction of γ’ precipitates reduced to 66,96% (±0,61) and 64,93% (±1,97) for 1500 and 2000 hours from 74,19% (±1,69)volume fraction in AS-HT sample. Therefore, these reduction in amount of γ’ precipitates showed that they started to dissolve into γ matrix.

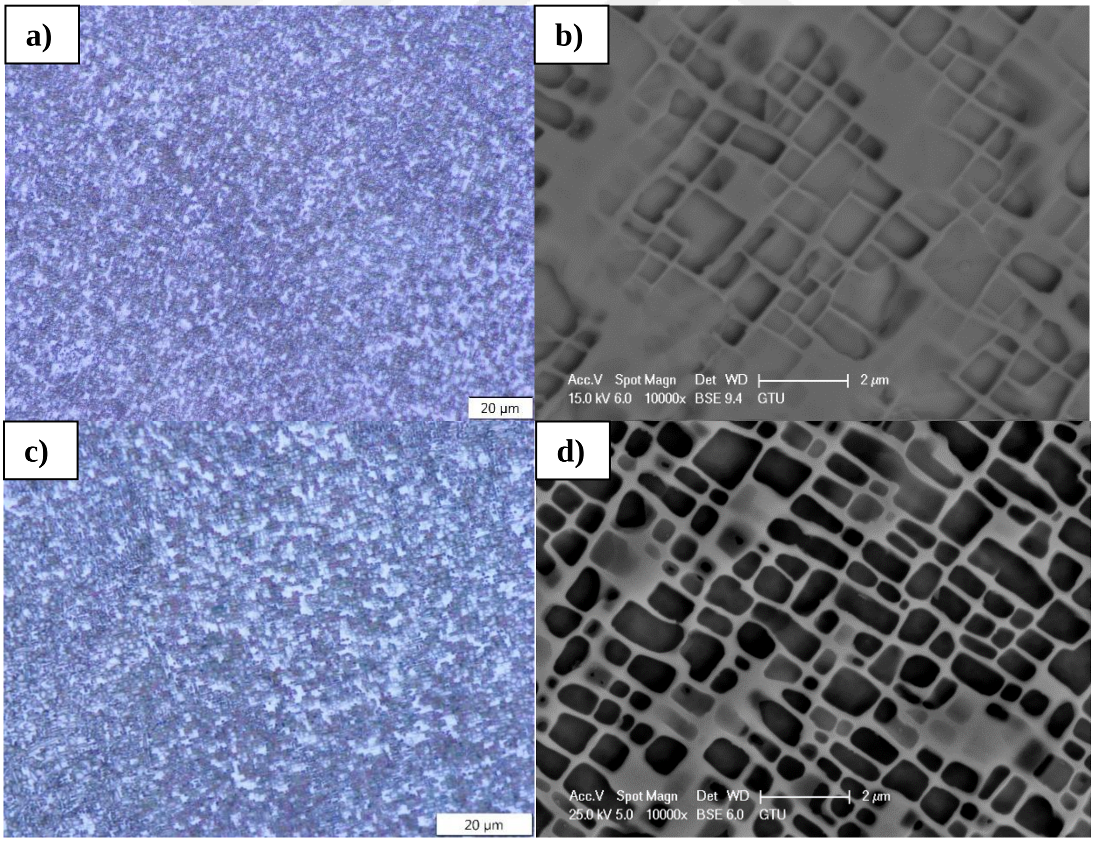

**Figure 3.4 :** Optical microscope images under 150x magnification and SEM images under 10000x magnification **(a)** and **(b)** after holding for 1500 hours, **(c)** and **(d)** after holding for 2000 hours at 980°C.

XRD patterns of 980ºC test bars consisted of one very strong, one intermediate and four smaller peaks (Figure 3.5) as observed in AS-HT sample. 2θ angles of peaks was very close to each other in XRD patterns of both samples whereas intensities of these peaks different from AS-HT sample. While strongest peak of sample held for 1500 hours at 50,86º had higher intensity than that of AS-HT sample, intensity of 2000 hours exposure sample at 50,90º was examined almost equal to highest intensity of AS-HT sample as shown in Figure 3.2 and Figure 3.5. Therefore, amount of γ and γ’ on [020] plane might have raise after 1500 hours but did not change after 2000 hours at 980ºC.

According to intensity ratios in Table 3.1 and Table 3.2, [030] and [040] peaks of these samples were stronger than that of AS-HT sample. [010] peak at 24,8º lost its intensity in 1500 hours exposure sample but it looked like steady in sample held for 2000 hours. [111] and [032] peaks kept their intensity ratios constant for both AS-HT sample and 980ºC samples. These results could be related with amouny of γ matrix and γ’ precipitates on those planes. Both [030] and [040] planes might have larger amount of γ’ particles and γ-γ’ phases in samples held at 980 for 1500 and 2000 hours than exist in AS-HT. [010] plane of sample held 1500 hours might have less γ’ precipitates while it might not change after 2000 hours on this plane.

**Table 3.2 :** 2θ angles and intensity ratios in XRD patterns of samples held at 980ºC for 1500 and 2000 hours.

| **Phase** | **1500 hours at 980 ºC** | | **2000 hours at 980 ºC** | |
|---|---|---|---|---|
| | 2θ angle (º) | Intensity ratio (%) | 2θ angle (º) | Intensity ratio (%) |
| **γ’ [010]** | 24,80 | 0,06 | 24,82 | 0,12 |
| **γ and γ’ [111]** | 45,64 | 0,12 | 45,66 | 0,13 |
| **γ and γ’ [200]** | 50,86 | 100,00 | 50,90 | 100,00 |
| **γ’ [030]** | 80,22 | 0,11 | 80,30 | 0,10 |
| **γ’ [032]** | 101,80 | 0,03 | 101,92 | 0,02 |
| **γ and γ’ [040]** | 118,44 | 17,20 | 118,60 | 13,28 |

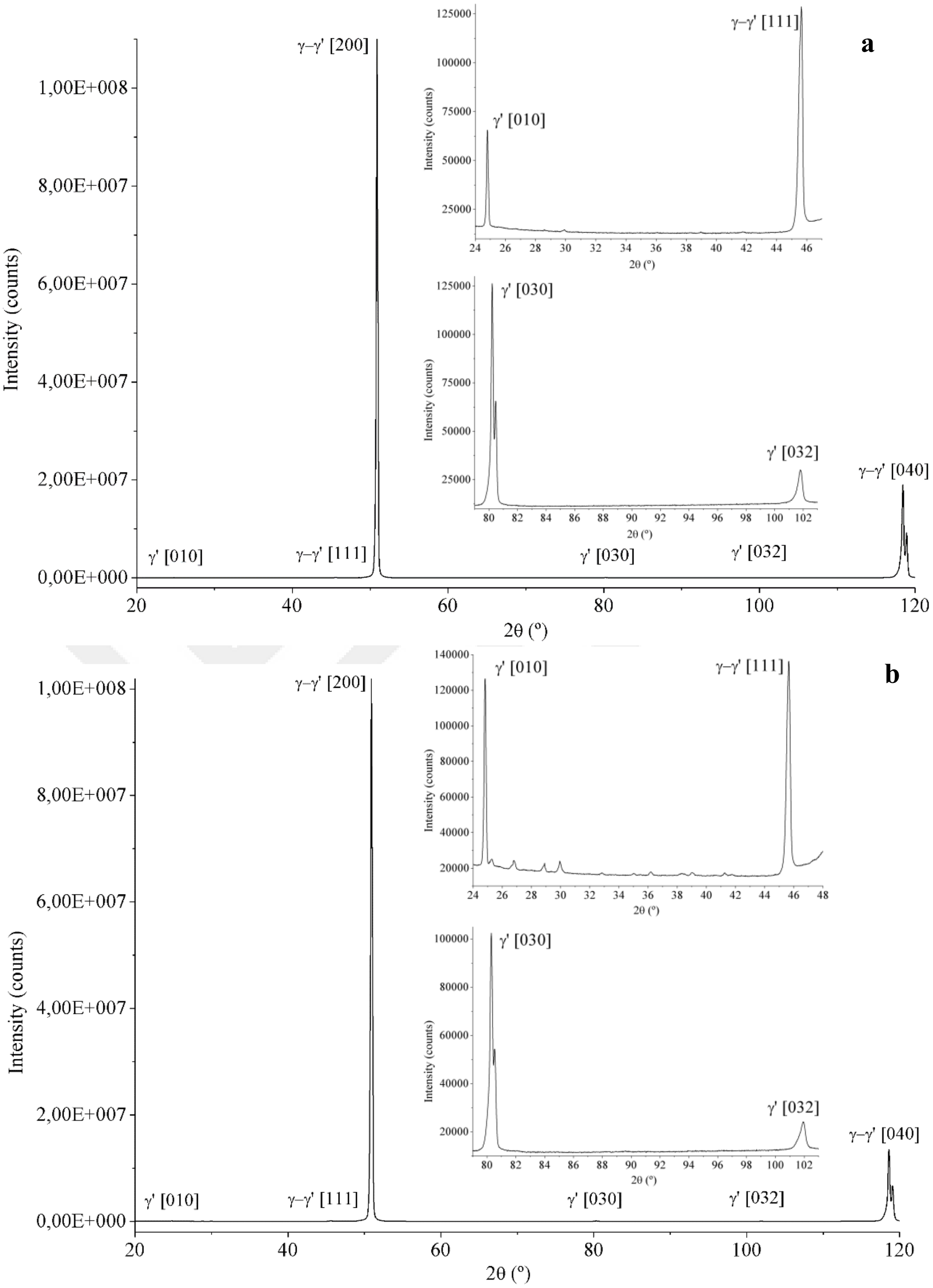

**Figure 3.5 :** XRD pattern of samples exposure to 980ºC for **(a)** 1500 and **(b)** 2000 hours.

TCP phases observed also in microstructures of both samples held for 1500 and 2000 hours unlike AS-HT sample. SEM micrographs and EDS analysis of TCP phases can be found in Figure 3.6 and Table 3.3. According to EDS results, TCP phases in both two test bars had very similar composition. There was slightly increases in Cr, Co, W and Re but decreases in Ni due to atomic percentages. According to atomic percentages, TCP in 1500 hours exporused sample might have $Cr_{12}Co_{15}W_7Re_6Ni_{60}$ whereas chemical formula of TCP in sample held for 2000 hours might be $Cr_{13}Co_{16}W_7Re_7Ni_{57}$. Therefore, TCP phases in two samples can be same TCP phase since chemical compositions were almost equal to each other. These TCP phases might be σ phase since it is rich in Ni and Cr and poor in W and Re as mentioned in study of Rae et.al [11]. However, expected phase to form was μ phase, which includes high W, low Cr, above 950ºC. Other evidence of σ phase was feathery like morphology after 1500 hours [11] but morphology adjusted to blocky shape after 2000 hours as shown in Figure 3.6 (a) and (b). This change in shape of TCP phases due to longer holding time was explained by Cheng et.al [16] for μ phase in single crystal alloy with 3,0 wt% Re. Therefore, σ phase may be affected in same way with μ phase by exposure time but there was no studies prove this estimation done in previous years.

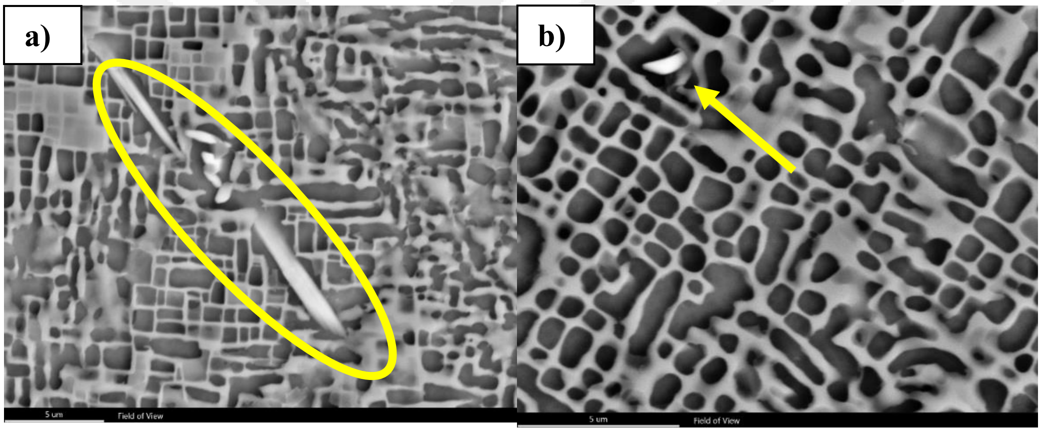

**Figure 3.6 :** SEM micrographs of TCP phases formed after **(a)** 1500 hours and **(b)** 2000 hours at 980°C with 5000x magnification.

**Table 3.3 :** EDS results of TCP phases after 1500 hours and 2000 hours at 980°C.

| **Element** | **Cr** | | **Co** | | **W** | | **Re** | | **Ni** | |
|---|---|---|---|---|---|---|---|---|---|---|
| | **wt%** | **at%** | **wt%** | **at%** | **wt%** | **at%** | **wt%** | **at%** | **wt%** | **at%** |
| **1500 hours at 980 ºC** | 8,63 | 12,28 | 11,56 | 14,52 | 17,72 | 7,13 | 14,14 | 5,62 | 47,95 | 60,44 |
| **2000 hours at 980 ºC** | 8,95 | 13,16 | 11,96 | 15,52 | 17,57 | 7,31 | 18,08 | 7,43 | 43,44 | 56,58 |

### 3.3 Structural Futures of Samples Held at 1100°C for 1500 and 2000 Hours

When the samples heated to 1100°C and held for 1500 hours, amount of increase in size of γ’ precipitates was much more than that of samples held at 980°C for 1500 and

2000 hours. Size of γ’ precipitates increased to 5,58 μm (±2,39) from 0,38 μm and percentange of the particles fall to 61,30% (±1,17) from 74,19%. Morphology of γ’ phases was completely broken and changed to rafting like shape Figure 3.1 (g and h) so they lost their homogenous cubic shape exist in AS-HT condition. And this rafting like coarsening occurred spontaneously in different directions since there was no applied force as found in research of Gebura and Lapin [45]. Furhermore, they became clearly distinguishable and detectable under optical microscope rather than SEM.

Then, test bars was continued to subjecting temperature of 1100°C up to 2000 hours and rafted like γ’ particles proceeded coarsening to 6,59 μm (±3,27) as can be seen in Figure 3.1.j. Also, Figure 3.1.i shows optical microscope image of γ’ phases in microstructure that was more visible than the other long time exposure samples. Volume fraction of γ’ precipitates had very sharp decreases to 54,19% (±1,39) according to other samples.

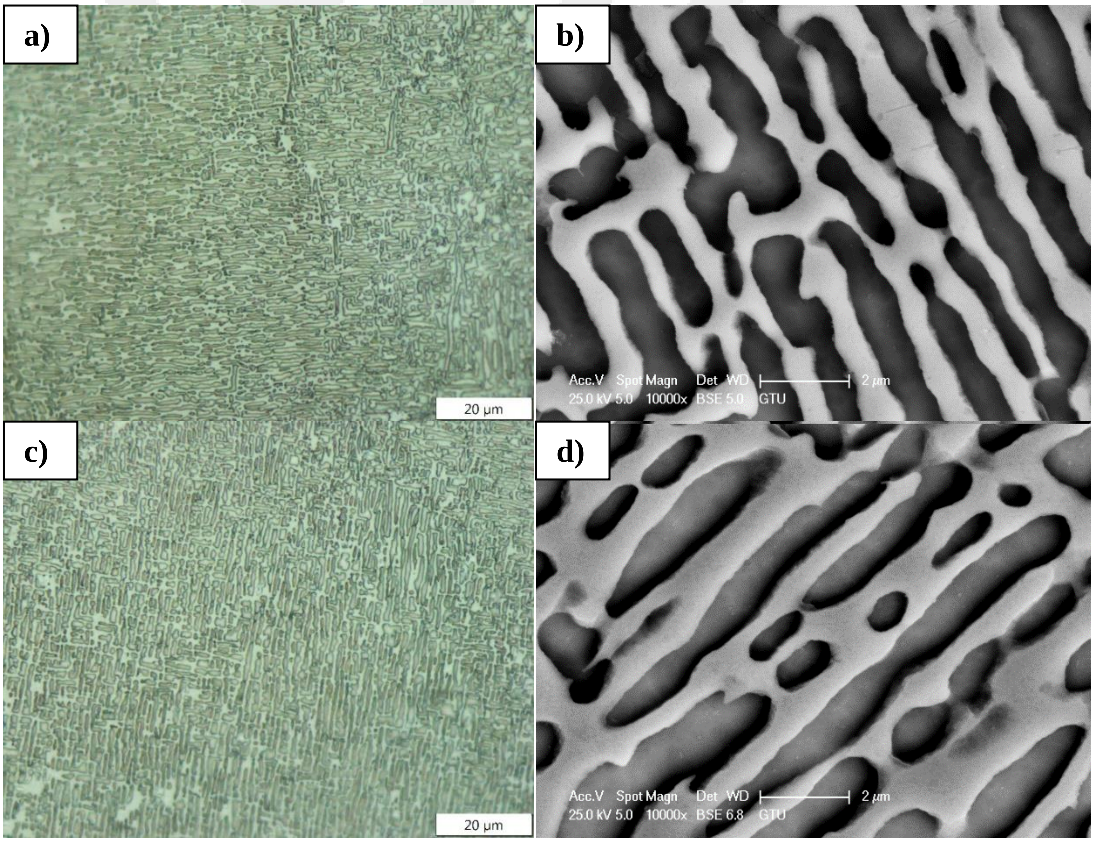

**Figure 3.7 :** Optical microscope images under 150x magnification and SEM images under 10000x magnification **(a)** and **(b)** after holding for 1500 hours, **(c)** and **(d)** after holding for 2000 hours at 1100°C.

Subjecting samples to 1100ºC for 1500 and 2000 hours had also some effects on XRD patterns like effects of temperature of 980ºC. [010] and [111] peaks, lost their intensities according to AS-HT sample as given in Table 3.1 and Table 3.4 like strongest [020] peak. It had intensity of 100 million counts (Figure 3.2) but it decreased to 93 million counts in sample held for 1500 hours and significantly to 67 millions in sample held for 2000 hours at 1100ºC (Figure 3.8). On the contrary, intensity ratios of [040] peak at 118º increased in both 1500 and 2000 exposure samples comparing to that of AS-HT sample. Furthermore, [030] and [032] peak ratios was not affected from temperature and time. Therefore, [020] plane might less amount of γ-γ' phase while γ-γ'phase could be existed on [040] plane in samples held at 1100ºC for 1500 and 2000 hours according to AS-HT sample. γ' precipitate did not probably changed on [030] and [032] but might be reduced on [111].

Intensities of [020] peaks in samples held at 1100ºC had lower values than that of samples exposure to 980ºC (Figure 3.5) similar to AS-HT. Peaks belongs to [010] and [040] had also less intensity ratios in patterns of samples held at 1100ºC. Yet, intensity ratios of other peaks, [111], [030] and [032], have stayed stable according to that of samples held at 980ºC. As a result, [020] and [040] planes might lose γ-γ'phase at higher temperatures, and γ' amount on [010] could also decrease.

In addition, there was a big difference between XRD patterns of test bars held for 1500 hours and 2000 hours at 1100ºC, especially in intensities of two main peaks; [020] and [040]. [020] peak intensity reduced extremely from 9,3 million counts to 6,7 milllions as shown in Figure 3.8 and [040] peak ratio had higher value in sample held for 1500 hours (Table 3.4). However, both two samples had equal intensity ratio on [010], [111], [030] and [032] planes as given in Table 3.4. So it can be said that amount of γ-γ'phase might be decrease with increase in holding time at 1100ºC on [020] and [040] planes and no change in other four planes belongs to just γ' phase.

**Table 3.4 :** 2θ angles and intensity ratios in XRD patterns of samples held at 1100ºC for 1500 and 2000 hours.

| Phase | 1500 hours at 1100 ºC | | 2000 hours at 1100 ºC | |
|---|---|---|---|---|
| | 2θ angle (º) | Intensity ratio (%) | 2θ angle (º) | Intensity ratio (%) |
| **γ' [010]** | 25,06 | 0,03 | 24,78 | 0,03 |
| **γ and γ' [111]** | 45,92 | 0,13 | 45,62 | 0,12 |
| **γ and γ' [200]** | 51,18 | 100 | 50,86 | 100 |
| **γ' [030]** | 80,58 | 0,09 | 80,24 | 0,07 |
| **γ' [032]** | 102,08 | 0,03 | 101,72 | 0,03 |
| **γ and γ' [040]** | 118,80 | 11,63 | 118,44 | 5,16 |

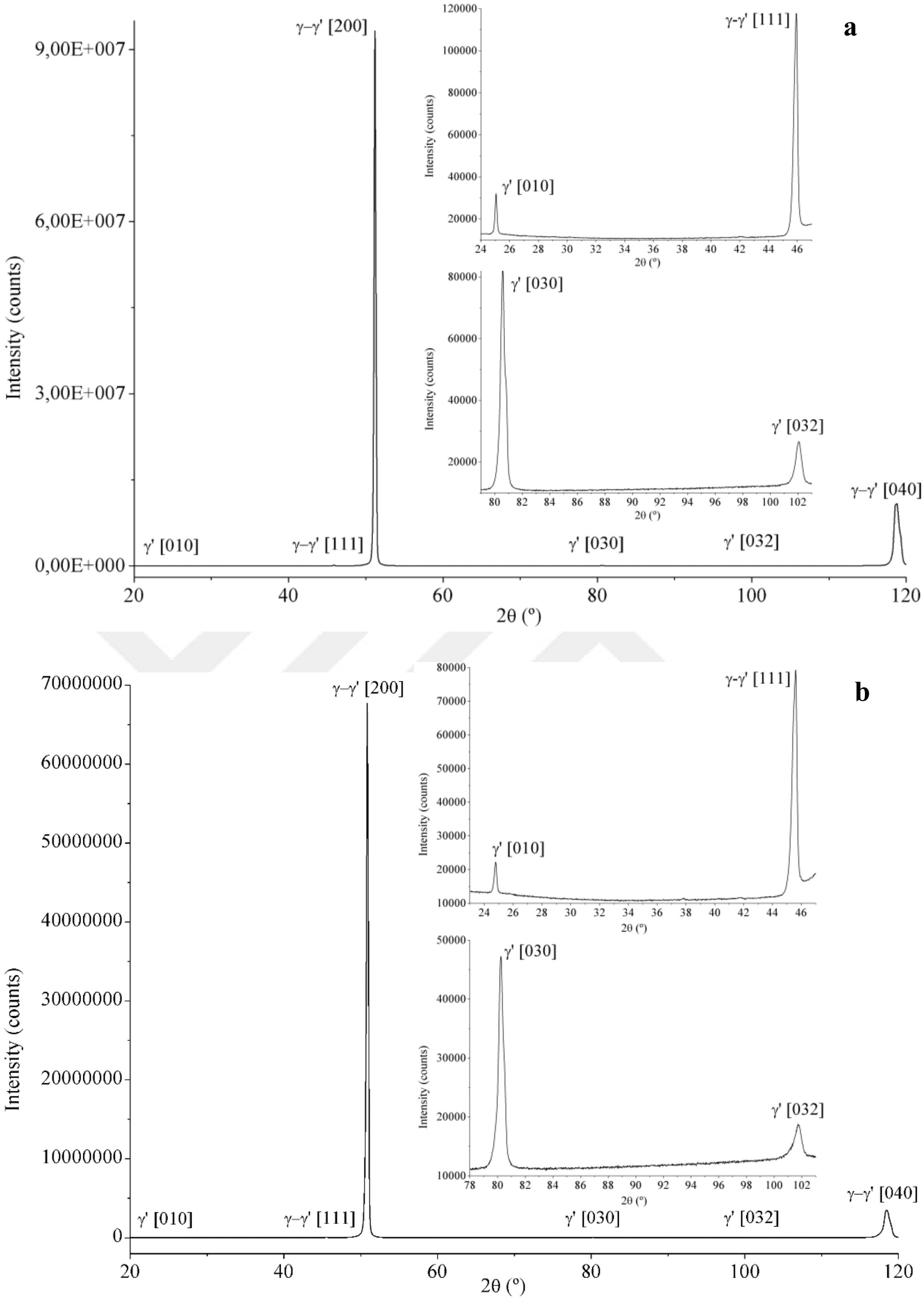

**Figure 3.8 :** XRD pattern of samples exposure to 1100ºC for **(a)** 1500 and **(b)** 2000 hours.

In addition, TCP phases found in both test bars at 1100ºC under SEM. TCP phases in both two samples had blocky shape as shown in Figure 3.9 (a) and (b) but they had different chemical composition from 980ºC. Ni decrased to 28 at% from 60 at% and

Co remained almost constant with 15 at% (Table 3.5). However, increase in compositions of W and Re was very high, and Cr content of TCPs also increased but not as much as that of W and Re. W content in 1100ºC samples raised by twice and amout of Re increased by three times in at% according to 980ºC samples as given in Table 3.3. Furhermore, compositions of TCPs in sample held for 1500 and 2000 hours had almost similar amount of elements so chemical formulas of TCPs might be $Cr_{20}Co_{15}W_{15}Re_{21}Ni_{28}$ at 1100ºC. EDS results in Table 3.5 was very similar to results obtained in studiy belongs to Dubiel et.al [46]who found that TCP phase consists of 35,9 Re, 30,9W, 10,3 Ni, 7,1 Co, 6,9 Cr in wt% after holding CMSX-4 single crystal alloy for 2500 hours at 1100ºC. Both Dubiel et.al [46] and Chmiela et.al [47] indicated also detected TCP phase was P phase held at 1100ºC for long time due to investigations under TEM. Therefore, examined TCP phase in this study can most probably be orthorhombic P phase according to EDS results.

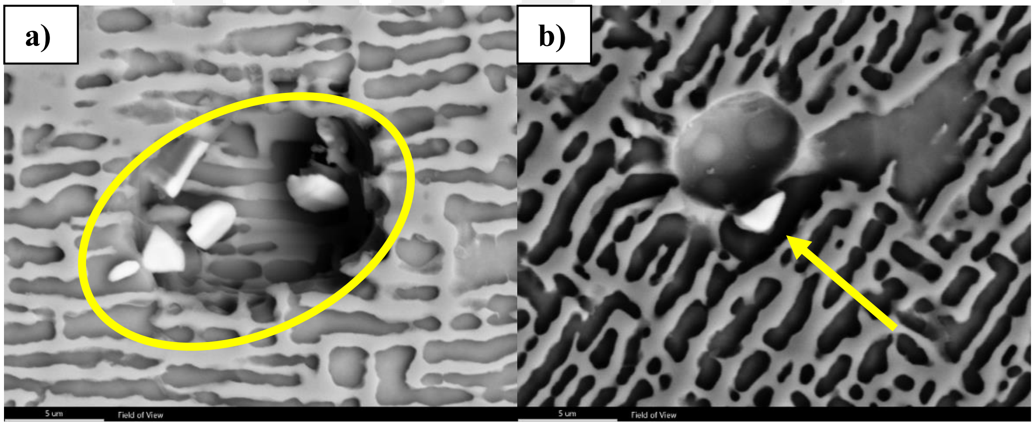

**Figure 3.9 :** SEM micrographs of TCP phases formed **(a)** 1500 hours and **(b)** 2000 hours at 1100°C with 5000x magnification.

**Table 3.5 :** EDS results of TCP phases after 1500 hours and 2000 hours at 1100°C.

| **Element** | **Cr** | | **Co** | | **W** | | **Re** | | **Ni** | |
|---|---|---|---|---|---|---|---|---|---|---|
| | **wt%** | **at%** | **wt%** | **at%** | **wt%** | **at%** | **wt%** | **at%** | **wt%** | **at%** |
| **1500 hours at 1100ºC** | 10,51 | 20,82 | 8,63 | 15,08 | 26,29 | 14,73 | 38,62 | 21,37 | 15,95 | 27,99 |
| **2000 hours at 1100ºC** | 9,67 | 19,08 | 9,63 | 16,76 | 27,97 | 15,6 | 36,4 | 20,04 | 16,32 | 28,51 |

## 3.4 High Temperature Tensile Testing

High temperature tensile testing graphs and results of the AS-HT samples and long-term exposed samples were given in Table 3.6 and stress-strain diagrams of the samples were given in Appendix E. These results showed that yield and tensile strength was 625 MPa and 833 after standard heat treatment, and the specimen elongated in length 34,50% and reduced in area of 38,70% due to initial length and area. Young's modulus of AS-HT sample was 93 GPA. In 1994, Sengupta and his colleagues [48] have investigated tensile behaviour of CMSX-4 single crystal alloy at different temperatures and they have found yield of 703 MPa, 811 MPa tensile strength and 82 GPa elastic modulus with 32,9% elongation after testing at 982ºC. Also Corrigan et.al [49] mentioned about 820 MPa ultimate tensile,  600 MPa yield strength, %18 elongation and 38% reduction in area at the same temperature to compare with new SX alloy invention in their patent. Therefore, tensile test results of samples in AS-HT condition (Table 3.6) was compatible with previous studies.

**Table 3.6 :** Tensile testing results of samples at 982ºC.

| | | **Elastic modulus (GPa)** | **Yield strength (MPa)** | **Tensile strength (MPa)** | **Elongation (%)** | **Reduction in area (%)** |
|---|---|---|---|---|---|---|
| **AS-HT** | **1** | 92,0 | 628,9 | 844,0 | 32,1 | 39,9 |
| | **2** | 94,6 | 622,9 | 822,7 | 36,9 | 37,5 |
| | **Avg** | 93,3 | 625,9 | 833,3 | 34,5 | 38,7 |
| **1500 hours at 980ºC** | **1** | 91,5 | 609,6 | 795,7 | 21,2 | 35,5 |
| | **2** | 89,4 | 596,0 | 779,8 | 27,5 | 42,4 |
| | **Avg** | 90,5 | 602,8 | 787,7 | 24,4 | 39,0 |
| **2000 hours at 980ºC** | **1** | 90,6 | 649,8 | 782,4 | 19,7 | 40,1 |
| | **2** | 89,9 | 649,8 | 782,4 | 21,3 | 38,5 |
| | **Avg** | 90,3 | 649,8 | 782,4 | 20,1 | 39,3 |
| **1500 hours at 1100ºC** | **1** | 85,2 | 564,2 | 717,8 | 21,9 | 46,5 |
| | **2** | 90,2 | 546,8 | 705,1 | 20,4 | 42,6 |
| | **Avg** | 87,7 | 555,5 | 711,4 | 21,1 | 44,5 |
| **2000 hours at 1100ºC** | **1** | 91,7 | 630,6 | 710,2 | 21,5 | 39,6 |
| | **2** | 90,0 | 598,4 | 709,9 | 18,6 | 36,5 |
| | **Avg** | 90,8 | 614,5 | 710,1 | 20,0 | 38,0 |

After heat applied at 980ºC for 1500 hours, tensile strength and elongation of the AS-HT specimens reduced to 787 MPa and 24 % (Table 3.6). Also, similar behaviour was observed after 2000 hours; tensile strength decreased to 782 MPa and 20% elongation was lower than elongation of AS-HT samples.Similar results was obtained in samples held at 1100ºC. After 1500 hours, tensile strength was 711 MPa and lower than that of both AS-HT and 980ºC samples as given in Table 3.6. Samples exposed to 1100ºC for 2000 hours had similar ultimate tensile with 1500 hours sample at 1100ºC, 710 MPa. Although, tensile strength was lost at 1100ºC, rupture strains were very close to results of samples held at 980ºC as seen in stress-strain diagrams of the sample in Appendix E. The reason of these reduction in tensile strength and elongation after 980 ºC and 1100 ºC might be the increase in size and changing the cubic shape of γ' precipitates due to AS-HT condition.

In addition these reduction in tensile strength, elastic modulus and reduction in area of the all samples did not change in positive or negative way. Also, TCP phases in long term exposure samples did not have any significant effect on high temperature strength due to its volume fraction in the microstructure of the samples.

Following the high temperature testing, fracture surfaces of both samples were examined, and digital microscope and SEM images were given below Figure 3.10-3.14 and Appendix F. At the first sight, cracks with various size under fracture surface can be easily detected on section view of all sample as shown in "a" sections of the figures below and App.F in macroscale. Most of these cracks were also perpendicular to direction of the tensile load. Then, it was observed that surface of the fractures had dull and rough appearance for both AS-HT and exposed samples in "b" section of the figures. To understand the fracture behavior, middle of the fracture surfaces were examined under SEM and dimples, which is a sign of typical ductile fracture behaviour [50], were seen clearly in SEM images (as marked in "c" sections of the figures). And according to SEM images, dimples were formed interfaces between γ' precipitates and γ matrix rather than grain boundaries since the samples had single crystal structure without any grain boundaries. Therefore, since fracture surfaces of all samples had dull and rough appereance, and contained dimples in the structure after high temperature tensile testing, it can be said that both samples had typical ductile fracture behavior.

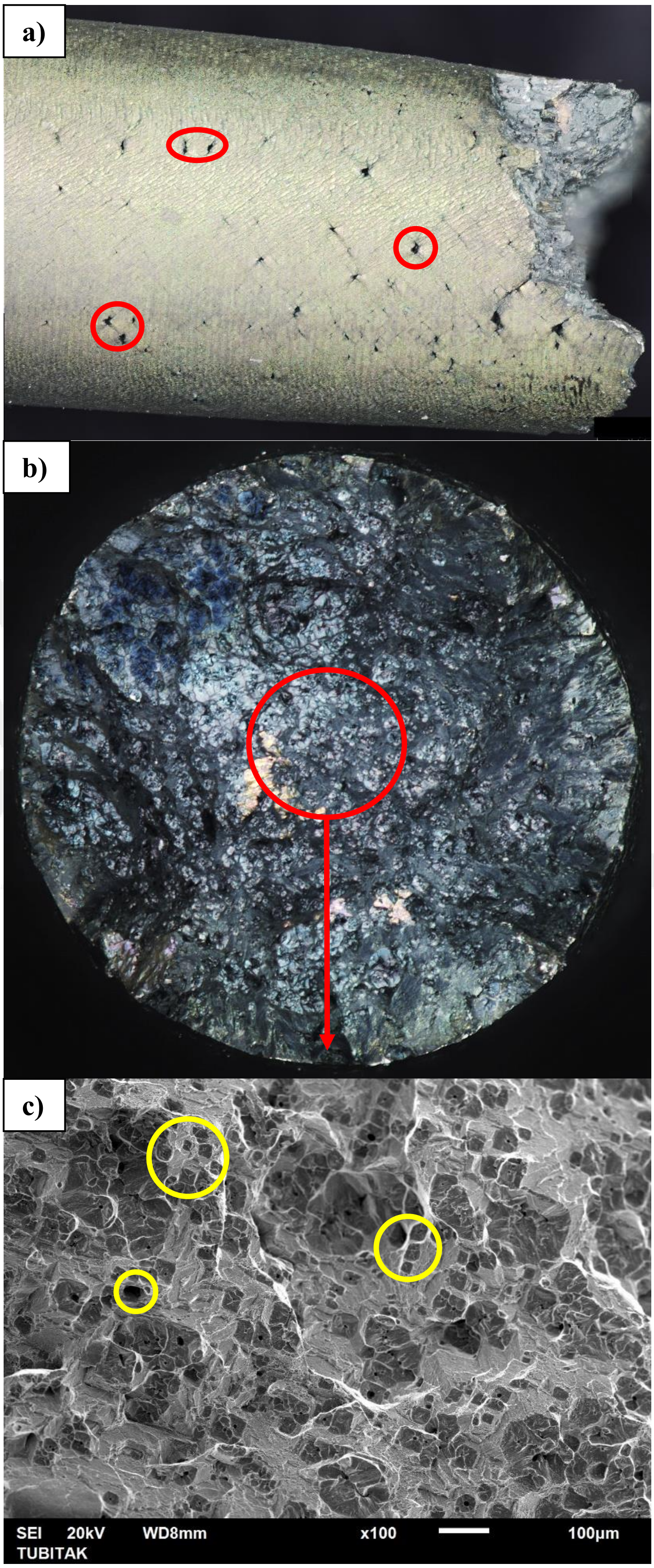

**Figure 3.10 :** **(a)** Cracks on section view of the fracture, **(b)** image of the fracture surface under digital microscope and **(c)** dimples on SEM image from middle of AS-HT sample.

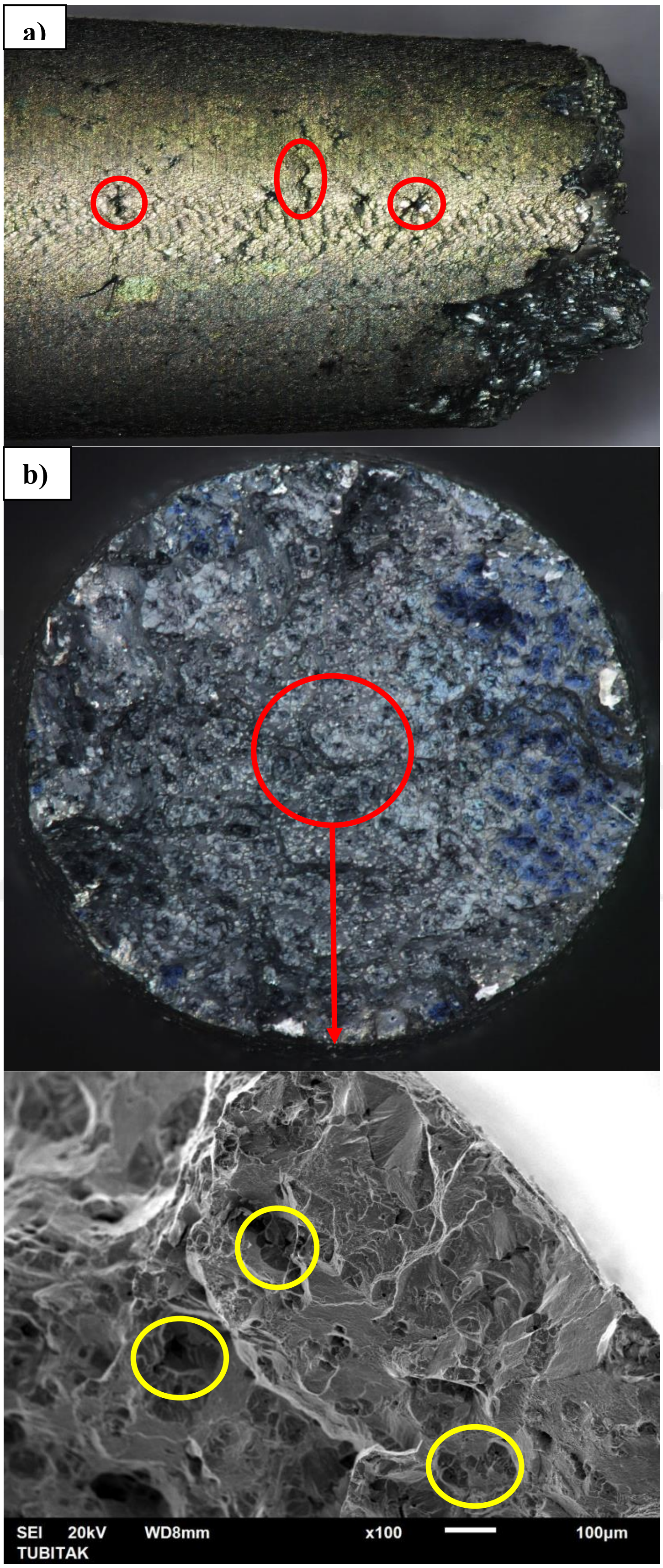

**Figure 3.11 : (a)** Cracks on section view of the fracture, **(b)** image of the fracture surface under digital microscope and **(c)** dimples on SEM image from middle of sample exposure to 980ºC for 1500 hours.

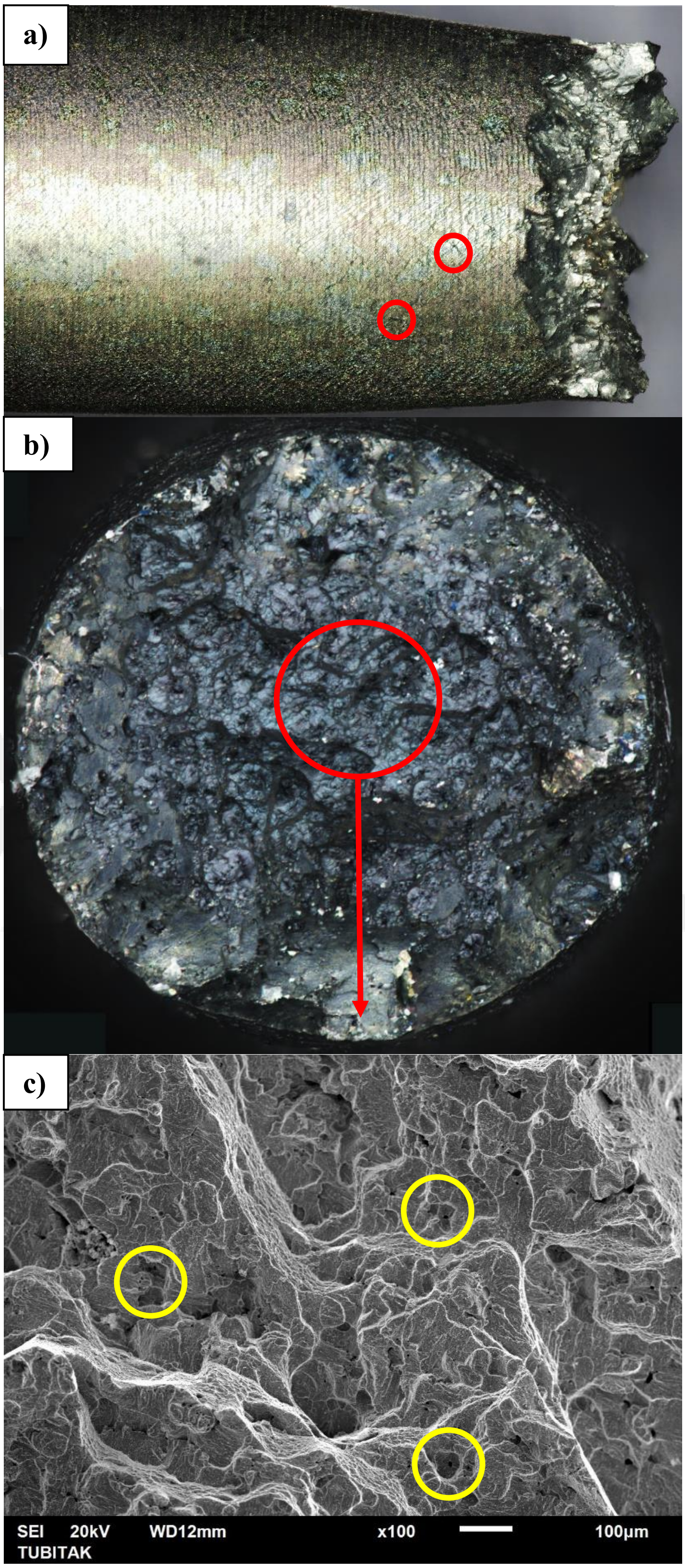

**Figure 3.12 : (a)** Cracks on section view of the fracture, **(b)** image of the fracture surface under digital microscope and **(c)** dimples on SEM image from middle of sample exposure to 980℃ for 2000 hours.

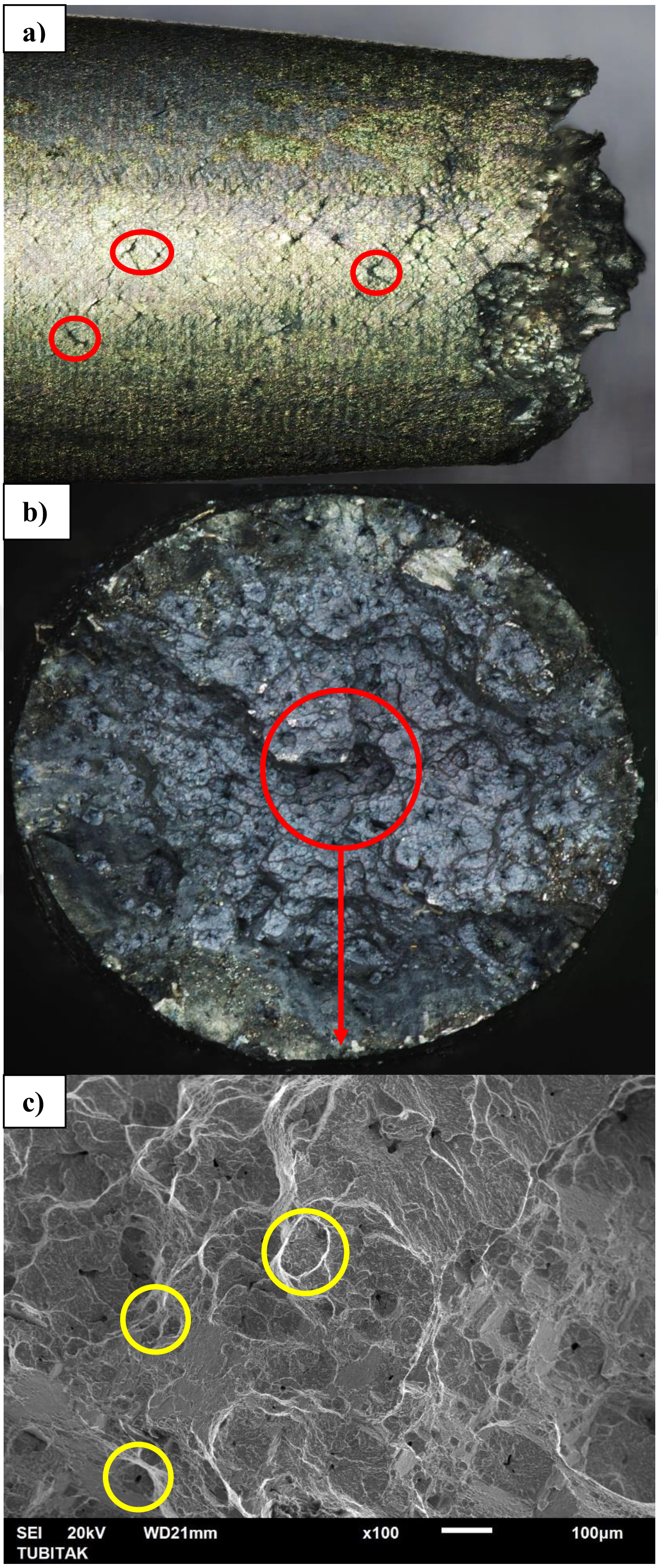

**Figure 3.13 :** **(a)** Cracks on section view of the fracture, **(b)** image of the fracture surface under digital microscope and **(c)** dimples on SEM image from middle of sample exposure to 1100ºC for 1500 hours.

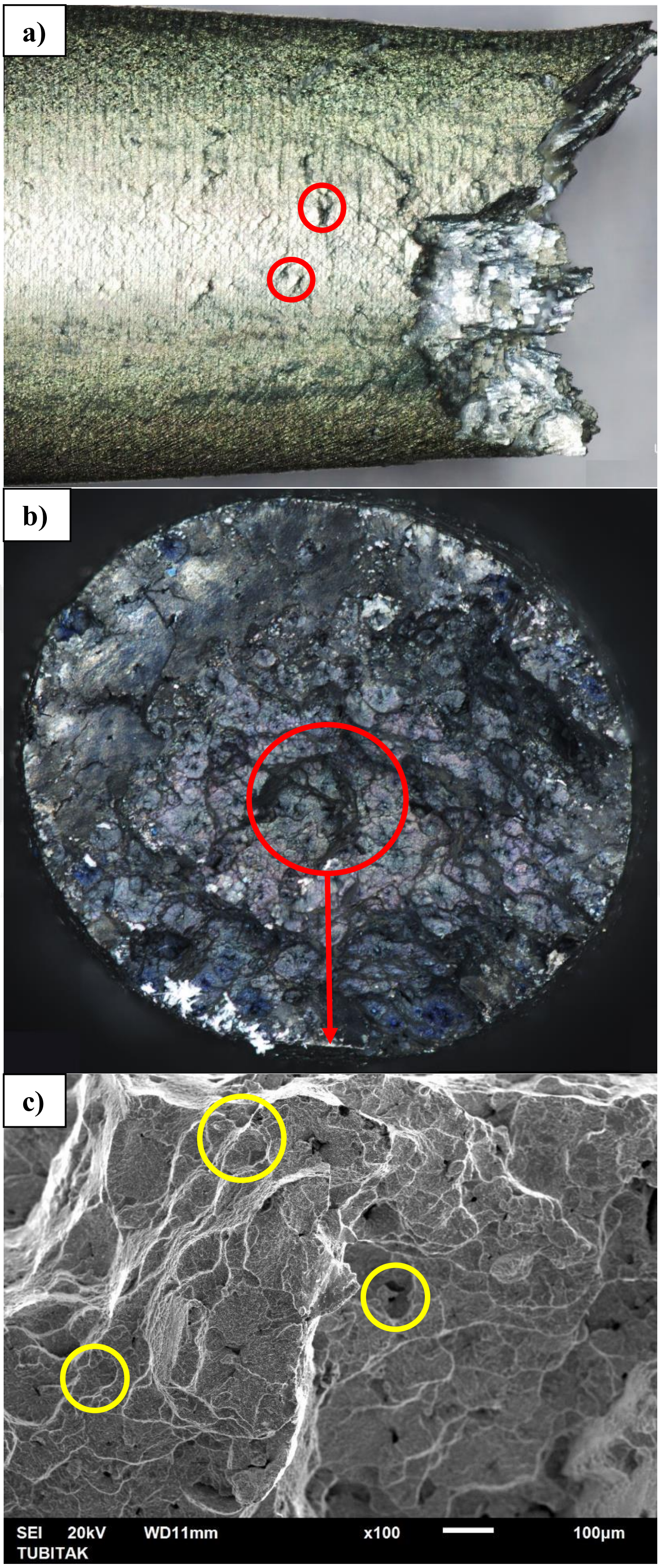

**Figure 3.14 : (a)** Cracks on section view of the fracture, **(b)** image of the fracture surface under digital microscope and **(c)** dimples on SEM image from middle of sample exposure to 1100ºC for 2000 hours.

# 4. CONCLUSIONS AND RECOMMENDATIONS

As a conclusion of this master thesis, nickel based superalloys, CMSX-4 SLS, test bars was first produced in single crystal form and standard heat treatment was applied to precipitate cubic γ’ phase on γ matrix. Then, test bars was subject to heat at 980ºC and 1100 ºC for 1500 and 2000 hours followed by structural and mechanical examinations.

- At 980ºC after 1500 hours, γ’ precipitates started to grow while preserving cubic morphology according to AS-HT condition. After 2000 hours, coarsening of the particles continued but they started to lose their cubic form. However, volume fraction of γ’ particles got lower from existing in AS-HT form so γ’ phase dissolved into γ matrix. Also, XRD patterns showed that amount γ and γ’ phases on some of the planes might have changed in samples held for long time to compare pattern of AS-HT sample.
- At 1100ºC, cubic morphology of γ’ precipitates has completely broken after holding for 1500 hours and 2000 hours. And size of γ’ phases was much higher than that of both AS-HT and 980ºC condition. The other change in microstructure was extremely decrease in volume fraction of γ’ particles according to after AS-HT and holding at 980ºC. Amount γ and γ’ phases on the planes might have differentiated according to both XRD patterns AS-HT sample and samples held 980ºC without any adjustment on 2θ angles of the phases due to XRD analysis results.
- According to tensile test results, the long term exposure samples was elongated less and had lower ultimate tensile strength than AS-HT sample. The reason might be related with changes of the shape and size of γ’ precipitates.
- Any significant effect of TCP phases on the strength could not be detected due to very low volume fraction of TCP phases.
- When fracture surfaces were examined, both samples showed typical ductile fracture behavior due to dull and rough surface on macroscale and dimples in SEM images.

The following further examinations can be studied as recommendations for future works:

- Changes in misfit between γ matrix and γ’ precipitates after long term exposure
- Creep and/or fatigue behavior of SX superalloy with coarsened γ’ precipitates and TCP phases formed at different temperatures and time
- TEM analysis TCP to determine exact phases.

# REFERENCES

[1] **Url-1** <https://www.rsc.org/periodic-table/element/28/nickel>, date retrieved 08.10.2020

[2] **Geddes, B., Leon, H., & Huang, X.** (2010). *Superalloys: Alloying and Performance*. ASM International.

[3] **Kracke, A.** (2010). Superalloys, the most successful alloy system of modern times - Past, present and future. In *7th International Symposium on Superalloy 718 and Derivatives 2010*.

[4] **Reed, R. C.** (2006). *The Superalloys fundamentals and applications*. New York: Cambridge University Press.

[5] **Donachie, M. J., & Donachie, S. J.** (2002). *Superalloys: A Technical Guide*. ASM International.

[6] **Cumpsty, N. A.** (1997). *Jet Repulsion: A Simple Guide to the Aerodynamic and Thermodynamic Design and Performance of Jet Engines*. Cambridge: Cambridge University Press.

[7] **Matuszewski, K.** (2016). *Precipitation of Topologically Close Packed Phases in Ni-base Superalloys – the Effect of Re and Ru* (Doctoral dissertation). Friedrich-Alexander University.

[8] **Sims, C. T., Stoloff, N. S., & Hagel, W. C.** (1987). Superalloys II. *Superalloys II*.

[9] **Koul, A. .** (1994). *Advances in High Temperature Structural Materials and Protective Coating*. Ottawa: National Research Council of Canada.

[10] **Boota, M., Gäbler, J., Schäfer, L., & Keunecke, M.** (2012). Investigations of suitable hard coatings on nickel-based single-crystal superalloy (CMSX-4). *Surface and Coatings Technology*, ***207***, 300–304.

[11] **Rae, C. M. F., Karunaratne, M. S. A., Small, C. J., Broomfield, R. W., Jones, C. N., & Reed, R. C.** (2000). Topologically Close Packed Phases in an Experimental Rhenium-Containing Single Crystal Superalloy. *Superalloys 2000*, 767–776. The Minerals, Metals & Materials Society.

[12] **Sinha, A. K.** (1972). Topologically close-packed structures of transition metal alloys. *Progress in Materials Science*, ***15***(2), 81-185.

[13] **Rae, C. M. F., & Reed, R. C.** (2001). The precipitation of topologically close-packed phases in rhenium-containing superalloys. *Acta Materialia*, ***49***(19), 4113-4125.

[14] **Graef, M. De, & McHenry, M. E.** (2007). *Structure of Materials: An Introduction to Crystallography, Diffraction, and Symmetry*. New York: Cambridge University Press.

[15] **Sugui, T., Minggang, W., Tang, L., Benjiang, Q., & Jun, X.** (2010). Influence

of TCP phase and its morphology on creep properties of single crystal nickel-based superalloys. *Materials Science & Engineering A*, ***527***(21–22), 5444–5451.

[16] **Cheng, K., Jo, C., Jin, T., & Hu, Z.** (2012). Effect of Re on the precipitation behavior of μ phase in several single crystal superalloys. *Journal of Alloys and Compounds*, ***536***, 7–19.

[17] **Cheng, K., Jo, C., Jin, T., & Hu, Z.** (2011). Precipitation behavior of μ phase and creep rupture in single crystal superalloy CMSX-4. *Journal of Alloys and Compounds*, ***509***, 7078–7086.

[18] **Dubiel, B., Indyka, P., Kruk, A., & Kalemba-Rec, I.** (2016). Characterisation of TCP phases in CMSX-4 single crystal superalloy subjected to high temperature annealing and creep deformation. *Inżynieria Materiałowa*, ***4***(212), 150–155.

[19] **Dubiel, B., Indyka, P., Moskalewicz, T., Kruk, A., Zubko, M., …Berent, K.** (2017). Characterization of the μ and P phase precipitates in the CMSX-4 single crystal superalloy. *Journal of Microscopy*, ***266***(3), 239–248. https://doi.org/10.1111/jmi.12532

[20] **Beeley, P. R., & Smart, R. F.** (1995). *Investment Casting*. London: The University Press Cambridge.

[21] **Simmonds, S.** (2013). *Formation and Avoidance of Surface Defects During Casting and Heat- Treatment of Single-Crystal Nickel- Based Superalloys* (Doctoral dissertation). University of Leicester.

[22] **Ma, D.** (2017). Novel casting processes for single-crystal turbine blades of superalloys. *Frontiers of Mechanical Engineering*, ***13***(1), 3-16.

[23] **Kubiak, K., Szeliga, D., Sieniawski, J., & Onyszko, A.** (2015). The Unidirectional Crystallization of Metals and Alloys (Turbine Blades). *Handbook of Crystal Growth*, 413-457.

[24] **Paraschiv, A., Matache, G., & Puscasu, C.** (2018). The effect of heat treatment on the homogenization of CMSX-4 Single-Crystal Ni-Based Superalloy. *Transportation Research Procedia*, ***29***, 303–311.

[25] **Szczotok, A.** (2013). On γ-γ ’ eutectic quantitative evaluation in the as-cast CMSX-4 nickel-based superalloy. *Solid State Phenomena*, ***197***, 203–208.

[26] **Wang, S.** (2005). *Welding and Repair of Single Crystal Ni-based Superalloys* (Master’s thesis). Carleton University.

[27] **Wilson, B. C., Hickman, J. A., & Fuchs, G. E.** (2003). The Effect of Solution Heat Treatment on a Single-Crystal Ni-Based Superalloy. *High Temperature Alloys*, ***55***(3), 35–40.

[28] **Aslan, O.** (2010). *Numerical modeling of fatigue crack growth in single crystal nickel based superalloys* (Doctoral dissertation). Paris Institute of Technology.

[29] **Durand-Charre, M.** (1997). *The Microstructure of Superalloys*. CRC Press.

[30] **Kakehi, K.** (1999). Influence of secondary precipitates and crystallographic orientation on the strength of single crystals of a Ni-based superalloy. *Metallurgical and Materials Transactions A*, ***30,*** 1249-1259.

[31] **Ricks, R. A., Porter, A. J., & Ecob, R. C.** (1983). The growth of gamma prime precipitates in nickel-base superalloys. *Acta Materiallurgica*, ***31***, 45–53.

[32] **Segersäll, M.** (2013). *Nickel-Based Single-Crystal Superalloys - the crystal orientation influence on high temperature properties* (Licentiate thesis). Linköping University.

[33] **Lall, C., Chin, S., & Pope, D. P.** (1979). The orientation and temperature dependence of the yield stress of Ni3 (Al, Nb) single crystals. *Metallurgical Transactions A*, ***10***(9), 1323–1332.

[34] **Feller-Kniepmeier, M., Link, T., Poschmann, I., Scheunemann-Frerker, G., & Schulze, C.** (1996). Temperature dependence of deformation mechanisms in a single crystal nickel-base alloy with high volume fraction of γ′ phase. *Acta Materialia*, ***44***(6), 2397–2407.

[35] **Matan, N., Cox, D. C., Rist, M. A., Rae, C. M. F., & Reed, R. C.** (1999). Creep of CMSX-4 superalloy single crystals: effects of misorientation and temperature. *Acta Materialia*, ***47***(5), 1549-1563.

[36] **Reed, R. C., Matan, N., Cox, D., Rist, M., & Rae, C. M.** (1999). Creep of CMSX-4 superalloy single crystals: effects of rafting at high temperature. *Acta Materialia*, ***47***(12), 3367–3381.

[37] **Goodlet, B. R., Rettberg, L. H., & Pollock, T. M.** (2016). Resonant ultrasound spectroscopy for defect detection in single crystal superalloy castings. In *Proceedings of the International Symposium on Superalloys*.

[38] **Cullity, B. D., & Stock, S. R.** (2001). *Elements of X-ray diffraction, 3rd edition*. Prentice Hall.

[39] **Bogdanowicz, W.** (2013). Characterization of single-crystal turbine blades by X-ray diffraction methods. *Solid State Phenomena*, **203-204**, 63–66.

[40] **Url-2** <https://www.protoxrd.com/products/laue-single-crystal/laue-cos>, date retrieved 08.10.2020

[41] **ASTM** (2010). *Standard Test Methods for Tension Testing of Metallic Materials* (ASTM E8/E8M).

[42] **Murakumo, T., Kobayashi, T., Koizumi, Y., & Harada, H.** (2004). Creep behaviour of Ni-base single-crystal superalloys with various γ′ volume fraction. *Acta Materialia*, ***52***(12), 3737-3744.

[43] **Url-3** <https://www.phase-trans.msm.cam.ac.uk/2003/Superalloys/superalloys.html>, date retrieved 21.07.2020

[44] **Bai, M.** (2015). *Fabrication and Characterization of Thermal Barrier Coatings* (Doctoral dissertation). University of Manchester.

[45] **Gebura, M., & Lapin, J.** (2008). Morphological changes of γ′ in Ni-based superalloy during long-term ageing. *17th International Metallurgical and Materials Conference, METAL 2008 - Proceedings*, 13–15.

[46] **Dubiel, B., Indyka, P., Kalemba-Rec, I., & Moskalewicz, T.** (2016). Analytical electron microscopy investigation of topologically close-packed phases in CMSX-4 single crystal superalloy. *Acta Physica Polonica A*, ***130***(4), 1110–1113.

[47] **Chmiela, B., Sozańska, M., & Rodak, K.** (2012). Phase identification in nickel-based superalloys using EBSD/SEM and electron diffraction in STEM. *Solid State Phenomena*, ***186***(2), 58–61.

[48] **Sengupta, A., Putatunda, S. K., Bartosiewicz, L., Hangas, J., Nailos, P. J., …Alberts, F. E.** (1994). Tensile behavior of a new single crystal nickel-based superalloy (CMSX-4) at room and elevated temperatures. *Journal of Materials Engineering and Performance*, ***3***(5), 664–672. https://doi.org/10.1007/BF02645265

[49] **Corrigan, J., Launsbach, M. G., & Mihalisin, J. R.** (2012). *U.S. Patent No. US8241560B2*. Washington, DC: U.S. Patent and Trademark Office.

[50] **Dieter, G. E.** (1988). *Mechanical metallurgy*. London: McGraw-Hill Book Company.

[51] **Pollock, T. M., & Tin, S.** (2006). Nickel-based superalloys for advanced turbine engines: Chemistry, microstructure, and properties. *Journal of Propulsion and Power*, ***22***(2), 361-374.

[52] **Kawagishi, K., Yeh, A., Yokokawa, T., Kobayashi, T., Koizumi, Y., & Harada, H.** (2012). Development of an Oxidation-Resistant High-Strength Sixth-Generation Single-crystal Superalloy. *Proceeding of the 12th International Symposium on Superalloys, Superalloys 2012*.

[53] **Davis, J. R.** (2000). *ASM Specialty Handbook: Nickel, Cobalt, and Their Alloys*. ASM International.

## APPENDICES

**APPENDIX A** Chemical compositions of nickel based superalloys

**APPENDIX B** Phases in nickel based superalloys

**APPENDIX C** Macrostructure of test bars

**APPENDIX D** Cyrstallographic pattern of test bars

**APPENDIX E** Stress-Strain diagrams of the samples

**APPENDIX F** Section View Fractured Samples

# **APPENDIX A** Chemical Compositions of Nickel Based Superalloys

**Table A.1 :** Chemical compositions of nickel based superalloys in weight percentage [51–53].

| Alloy | Cr | Co | Mo | W | Ta | Re | Ru | Al | Ti | C | Hf | Others | Ni |
|---|---|---|---|---|---|---|---|---|---|---|---|---|---|
| Mar-M246 | 8,3 | 10 | 0,7 | 10 | 3 | | | 5,5 | 1 | 0,14 | 1,5 | 0,05 Zr<br>0,02 B | bal. |
| Rene 80 | 14 | 9,5 | 4 | 4 | | | | 3 | 5 | 0,17 | | 0,03 Zr<br>0,02 B | bal. |
| IN713LC | 12 | | 4,5 | | | | | 5,9 | 0,6 | 0,05 | | 2 Nb<br>0,1 Zr<br>0,01 B | bal. |
| C1023 | 15,5 | 10 | 8,5 | | | | | 4,2 | 3,6 | 0,16 | | 0,16 Zr<br>0,01 B | bal. |
| IN792 | 12,6 | 9 | 1,9 | 4,3 | 4,3 | | | 3,4 | 4 | 0,09 | | 0,06 Zr<br>0,02 B | bal. |
| GTD111 | 14 | 9,5 | 1,5 | 3,8 | 2,8 | | | 3 | 4,9 | 0,1 | | 0,01 Zr<br>0,01 B | bal. |
| PWA 1480 | 10 | 6 | | 4 | 12 | | | 5 | 1,5 | | | | bal. |
| Rene N4 | 12,8 | 9 | 1,9 | 3,8 | 4 | | | 3,7 | 4,2 | | | 0,5 Nb | bal. |
| SRR99 | 8 | 5 | 0 | 10 | 3 | | | 5,5 | 2,2 | | | | bal. |
| AM1 | 8 | 6 | 2 | 6 | 9 | | | 5,2 | 1,2 | | | | bal. |
| AM3 | 8 | 6 | 2 | 5 | 4 | | | 6 | 2 | | | | bal, |
| CMSX-2 | 8 | 5 | 0,6 | 8 | 6 | | | 5,6 | 1 | | | | bal. |
| CMSX-3 | 8 | 5 | 0,6 | 8 | 6 | | | 5,6 | 1 | | 0,1 | | bal. |
| CMSX-6 | 10 | 5 | 3 | 0 | 2 | | | 4,8 | 4,7 | | 0,1 | | bal. |
| MC2 | 8 | 5 | 2 | 8 | 6 | | | 5 | 1,5 | | | | bal. |
| CMSX-4 | 6,5 | 9 | 0,6 | 6 | 6,5 | 3 | | 5,6 | 1 | | 0,1 | 1 Zr | bal. |
| PWA 1484 | 6 | 10 | 2 | 6 | 9 | 3 | | 5,6 | 0 | | 0,1 | | bal. |
| SC180 | 5 | 10 | 2 | 5 | 8,5 | 3 | | 5,2 | 1 | | 0,1 | | bal. |
| LEK94 | 5,8-6,4 | 7,2-7,8 | 1,7-2,3 | 3-7 | 2-2,6 | 2,3-2,6 | | 6,2-6,8 | 0,9-1,1 | | 0,05-0,15 | | bal. |
| ReneN5 | 7 | 7,5 | 1,5 | 5 | 6,5 | 3 | | 6,2 | 0 | 0,05 | 0,15 | 0,01 Y | bal. |
| CMSX10 | 2 | 2 | 0,4 | 5 | 8 | 6 | | 5,7 | 0,2 | | 0,03 | 0,1 Nb | bal. |
| ReneN6 | 4,2 | 12,5 | 1,4 | 6 | 7,2 | 5,4 | | 5,7 | 0 | | 0,15 | 0,1 Nb<br>0,05 B<br>0,01 Y | bal. |
| RR2100 | 2,5 | 12 | 0 | 9 | 5,5 | 6,4 | | 6 | 0 | | 0 | | bal. |
| TMS75 | 3 | 12 | 2 | 6 | 6 | 5 | | 6 | 0 | | 0,1 | | bal. |
| MCNG | 4 | 0 | 1 | 5 | 5 | 4 | 4 | 5,2 | 1,1 | | 0 | | bal. |
| EPMI02 | 2 | 16,5 | 2 | 6 | 8,25 | 5,95 | 3 | 5,55 | 0 | | 0,15 | | bal. |
| RR2101 | 2,5 | 12 | 0 | 9 | 5,5 | 6,4 | 2 | 6 | 0 | | 0 | | bal. |
| TMS173 | 2,8 | 5,6 | 2,8 | 5,6 | 5,6 | 6,9 | 5 | 5,6 | 0 | | 0,1 | | bal. |
| TMS138 | 2,9 | 5,8 | 2,9 | 5,8 | 5,5 | 4,9 | | 5,8 | | | 0,1 | 3 lr | bal. |
| TMS162 | 2,9 | 5,8 | 3,9 | 5,8 | 5,6 | 4,9 | 6 | 5,8 | 0 | | 0,1 | | bal. |
| TMS196 | 4,6 | 5,6 | 2,4 | 5 | 5,6 | 6,4 | 5 | 5,8 | | | 0,1 | | bal. |
| TMS238 | 4,6 | 6,5 | 1,1 | 4 | 7,6 | 6,4 | 5 | 5,9 | 0 | | 0,1 | | bal. |
| IN718 | 19 | | 3 | | | | | 0,5 | 0,9 | | | 5,1 Nb<br>0,02 B | bal. |
| Rene41 | 19 | 11 | 10 | | | | | 1,5 | 3,1 | | | 0,005 B | bal. |
| Nimonic 80A | 19,5 | | | | | | | 1,4 | 2,4 | | | 0,06 Zr<br>0,003 B | bal. |
| Waspaby | 19,5 | 13,5 | 4,3 | | | | | 1,3 | 3 | | | 0,006 B | bal. |
| U720 | 17,9 | 14,7 | 3 | 1,3 | | | | 2,5 | 5 | | | 0,03 Zr<br>0,03 B | bal. |

## **APPENDIX B** Phases in Nickel Based Superalloys

**Table B.1 :** Phases in nickel based superalloys [4, 5, 7, 13].

| **Phase** | **Crystal Structure** | **Space Group** | **Lattice Parameter (nm)** | **Chemical Formula** |
|---|---|---|---|---|
| γ | FCC | | | Ni |
| γ’ | FCC (ordered $L1_2$) | | $Ni_3Al$ to 0.3568 for $Ni_3(A1_{0.5}Ti_{0.5})$ | $Ni_3A1$<br>$Ni_3(A1, Ti)$ |
| γ’’ | BCT (ordered $D0_{22}$) | | $a_0 = 0.3624$<br>$c_0 = 0.7406$ | $Ni_3Nb$ |
| η | HCP ($D0_{24}$) | | $a_o = 0.5093$<br>$c_o = 0.8276$ | $Ni_3Ti$ |
| δ | Orthorhombic (ordered $Cu_3Ti$) | $P6_3/mmc$ | $a_o = 0.3624–0.511$<br>$b_0 = 0.421–0.4251$<br>$c_o = 0.452–0.4556$ | $Ni_3Nb$ |
| MC | Cubic | | $a_o = 0.430–0.470$ | TiC<br>NbC<br>HfC |
| $M_{23}C_6$ | FCC | | $a_o = 1.050–1.070$ | $Cr_{23}C_6$<br>$(Cr, Fe, W, Mo)_{23}C_6$<br>$Fe_3Mo_3C$ |
| $M_6C$ | FCC | | $a_0 = 1.085–1.175$ | $Fe_3W_3C$ $Fe_4W_2C$<br>$Fe_3Nb_3C$<br>$Nb_3Co_3C$<br>$Ta_3Co_3C$ |
| $M_7C_3$ | Hexagonal | | $a_o = 1.398$<br>$c_o = 0.4523$ | $Cr_7C_3$ |
| $M_3B_2$ | Tetragonal | | $a_o = 0.560–0.620$<br>$c_o = 0.300–0.330$ | $Ta_3B_2$<br>V3B2<br>$Nb_3B_2(Mo, Ti, Cr, Ni, Fe_3B_2)$<br>$Mo_2FeB_2$ |
| MN | Cubic | | $a_o = 0.4240$ | TiN<br>(Ti, Nb, Zr)N<br>(Ti, Nb, Zr)(C, N)<br>ZrN<br>NbN |
| σ | Tetragonal | $P4_2/mnm$ | $a_o = 0.880–0.910$<br>$c_o = 0.450–0.480$ | FeCr<br>FeCrMo<br>CrFeMoNi<br>CrCo<br>CrNiMo<br>$Cr_2Re_3$ |
| μ | Rhombohedral | R3m | $a_o = 0.475$<br>$c_o = 2.554$ | $Co_2W_6$<br>$(Fe, Co)_7(Mo, W)_6$<br>$W_6Co_7$ |
| P | Orthorhombic | Pnma | $a_0 = 1.72$<br>$b_0 = 0.48$<br>$c_0 = 0.91$ | $Cr_9Mo_{21}Ni_{20}$ |
| R | Rhombohedral | R3 | $a_0 = 1.09$<br>$c_0 = 1.93$ | $Cr_{18}Mo_{31}Co_{51}$<br>$Fe_{52}Mn_{16}Mo_{32}$ |

## **APPENDIX C** Macrostructure of Test Bars

**Figure C.1 :** Test bar no 1 after macroetching to observe single crystal structure.

**Figure C.2 :** Test bar no 2 after macroetching to observe single crystal structures.

,

**Figure C.3 :** Test bar no 3 after macroetching to observe single crystal structure.

**Figure C.4 :** Test bar no 4 after macroetching to observe single crystal structure.

**Figure C.5 :** Test bar no 5 after macroetching to observe single crystal structure.

**Figure C.6 :** Test bar no 6 after macroetching to observe single crystal structure.

**Figure C.7 :** Test bar no 7 after macroetching to observe single crystal structure.

**Figure C.8 :** Test bar no 8 after macroetching to observe single crystal structure.

# APPENDIX D Cyrstallographic Patterns of Test Bars

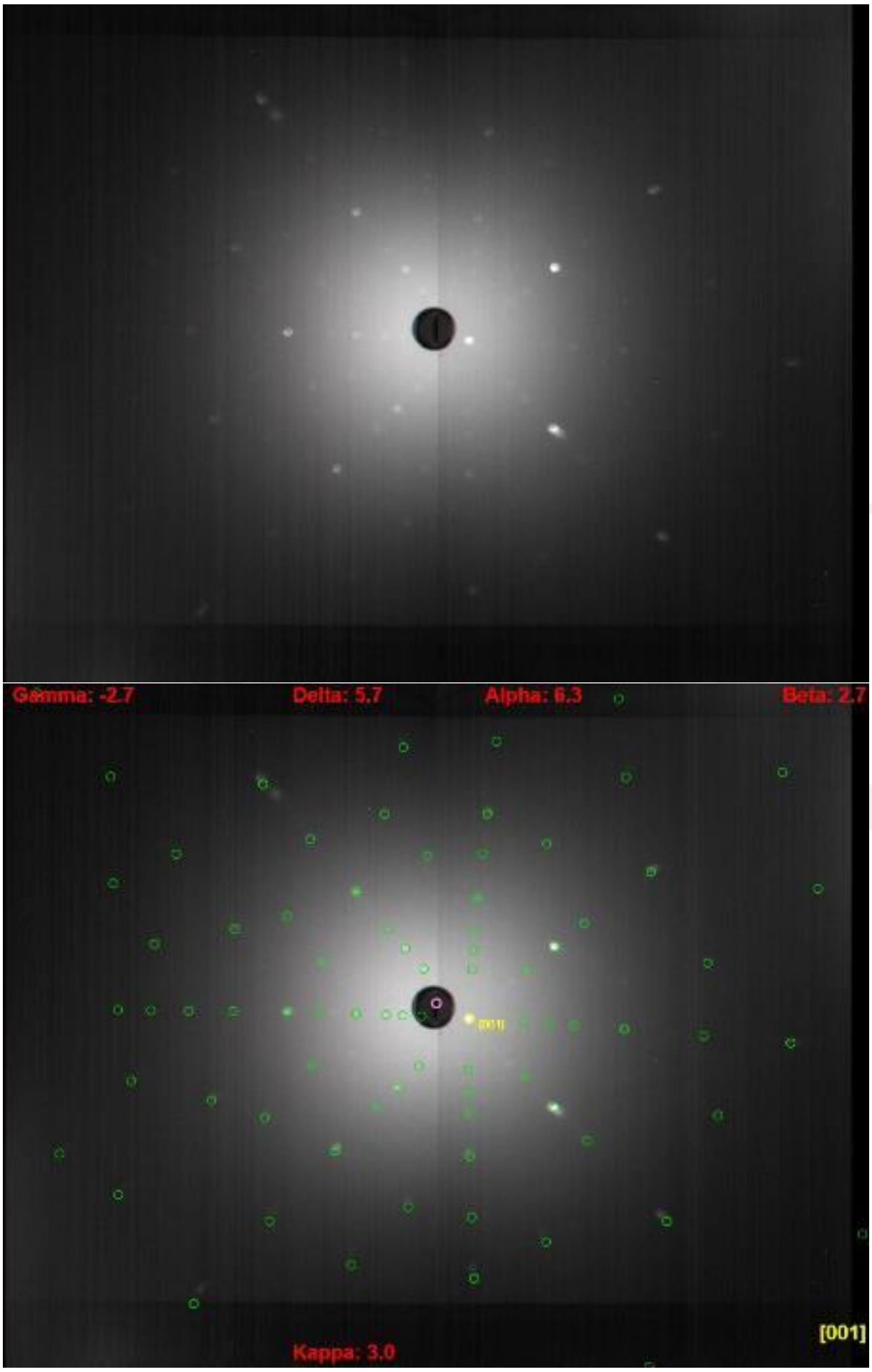

**Figure D.1 :** Laue pattern of test bar number 1.

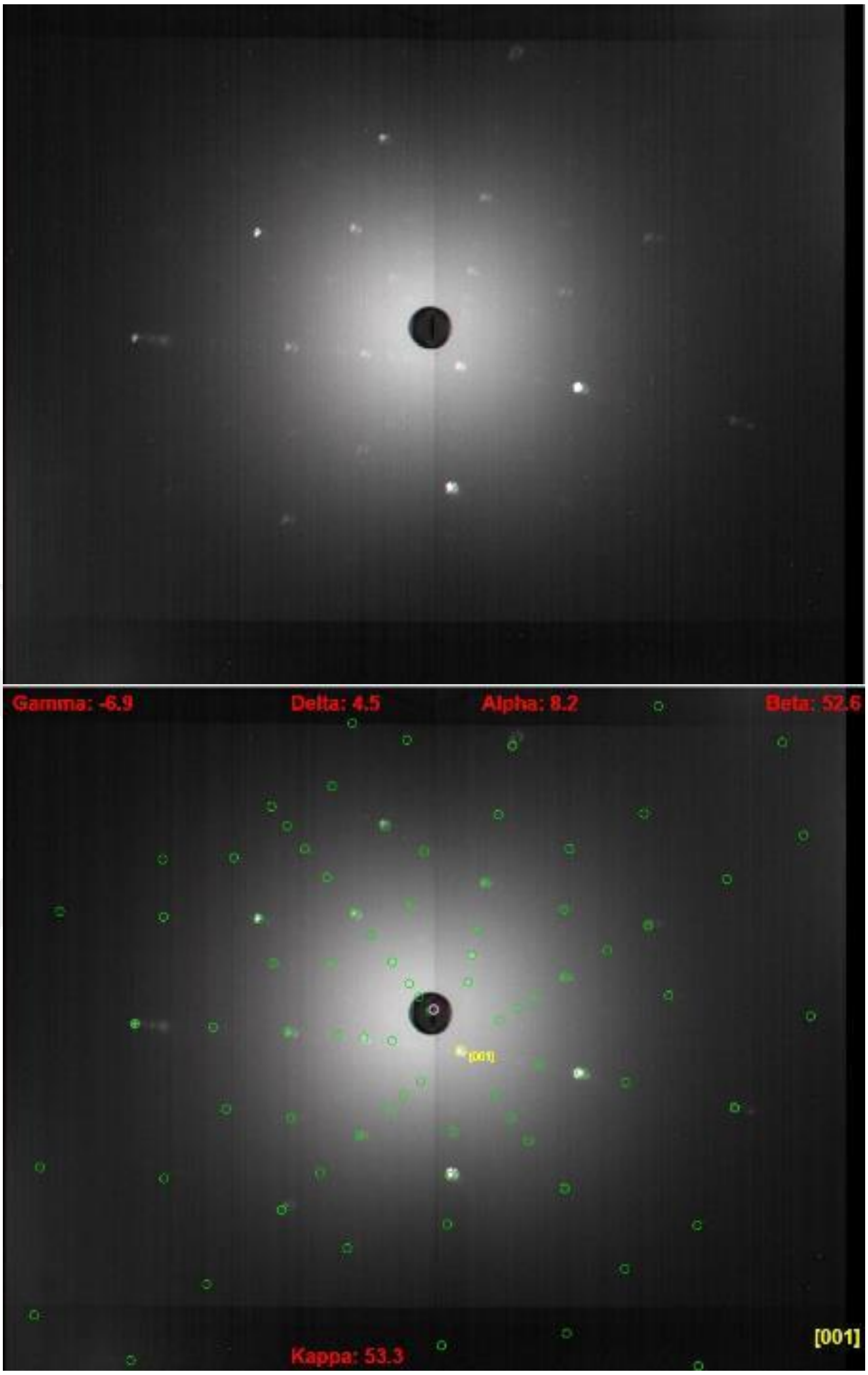

**Figure D.2 :** Laue pattern of test bar number 2.

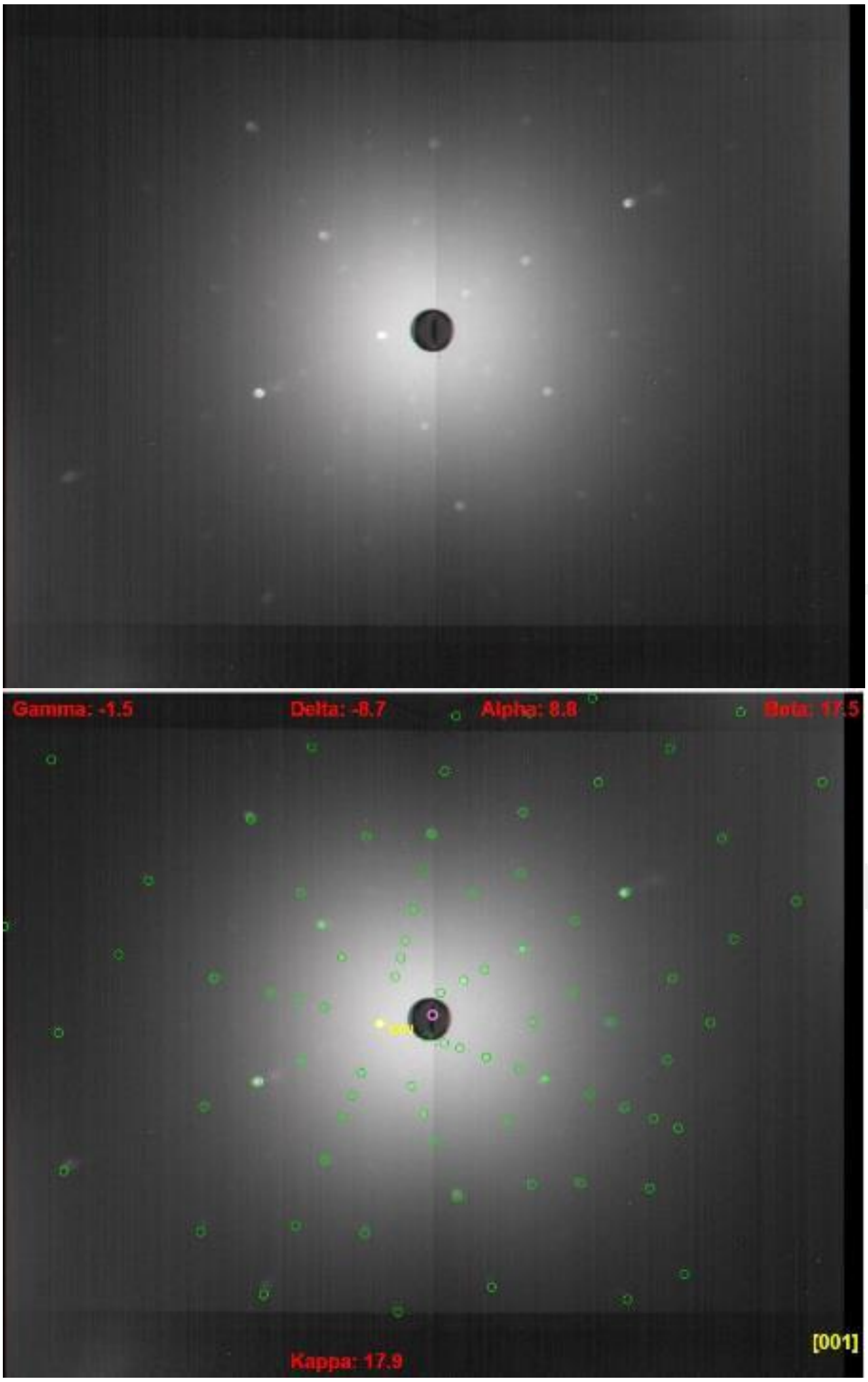

**Figure D.3 :** Laue pattern of test bar number 3.

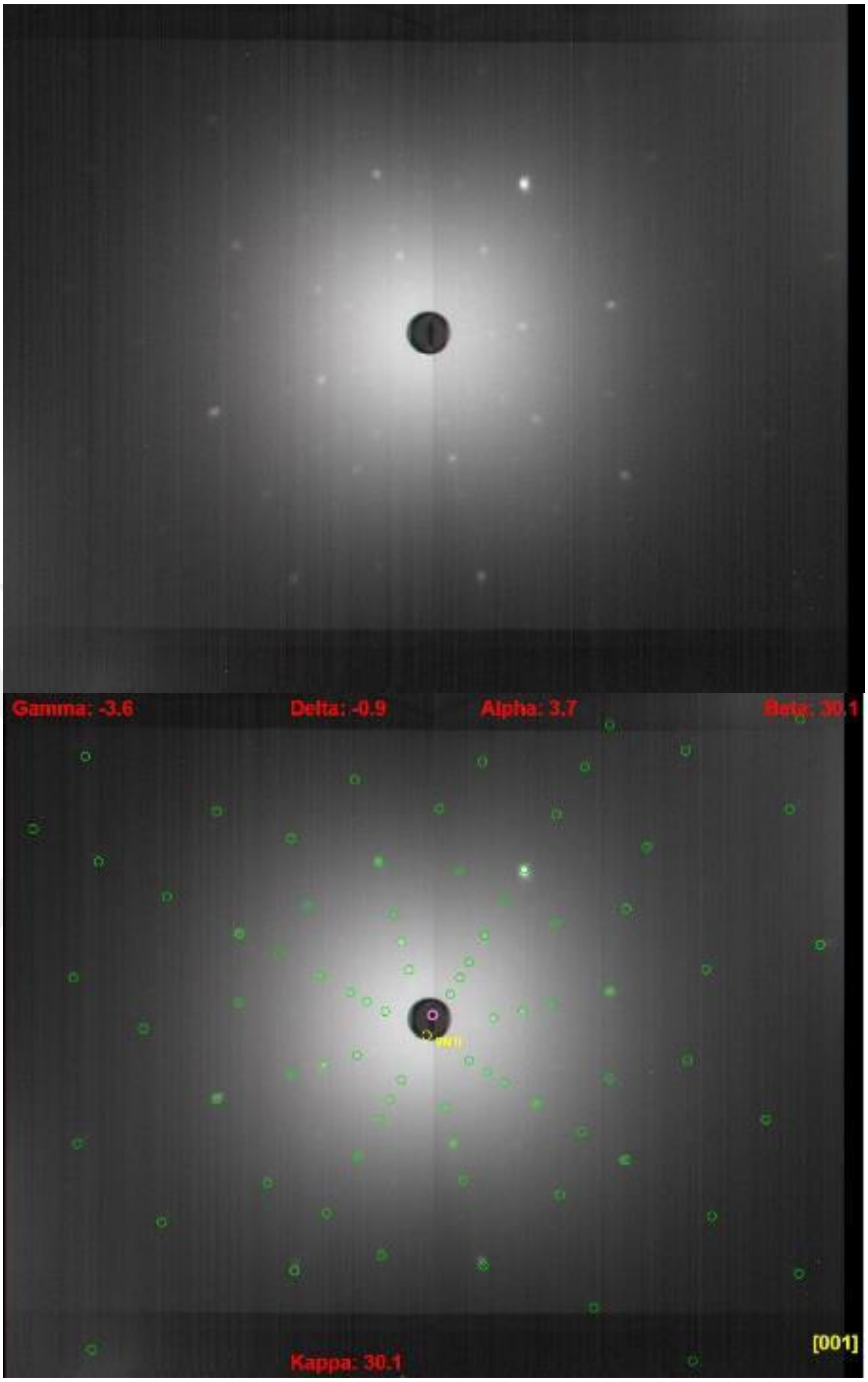

**Figure D.4 :** Laue pattern of test bar number 4.

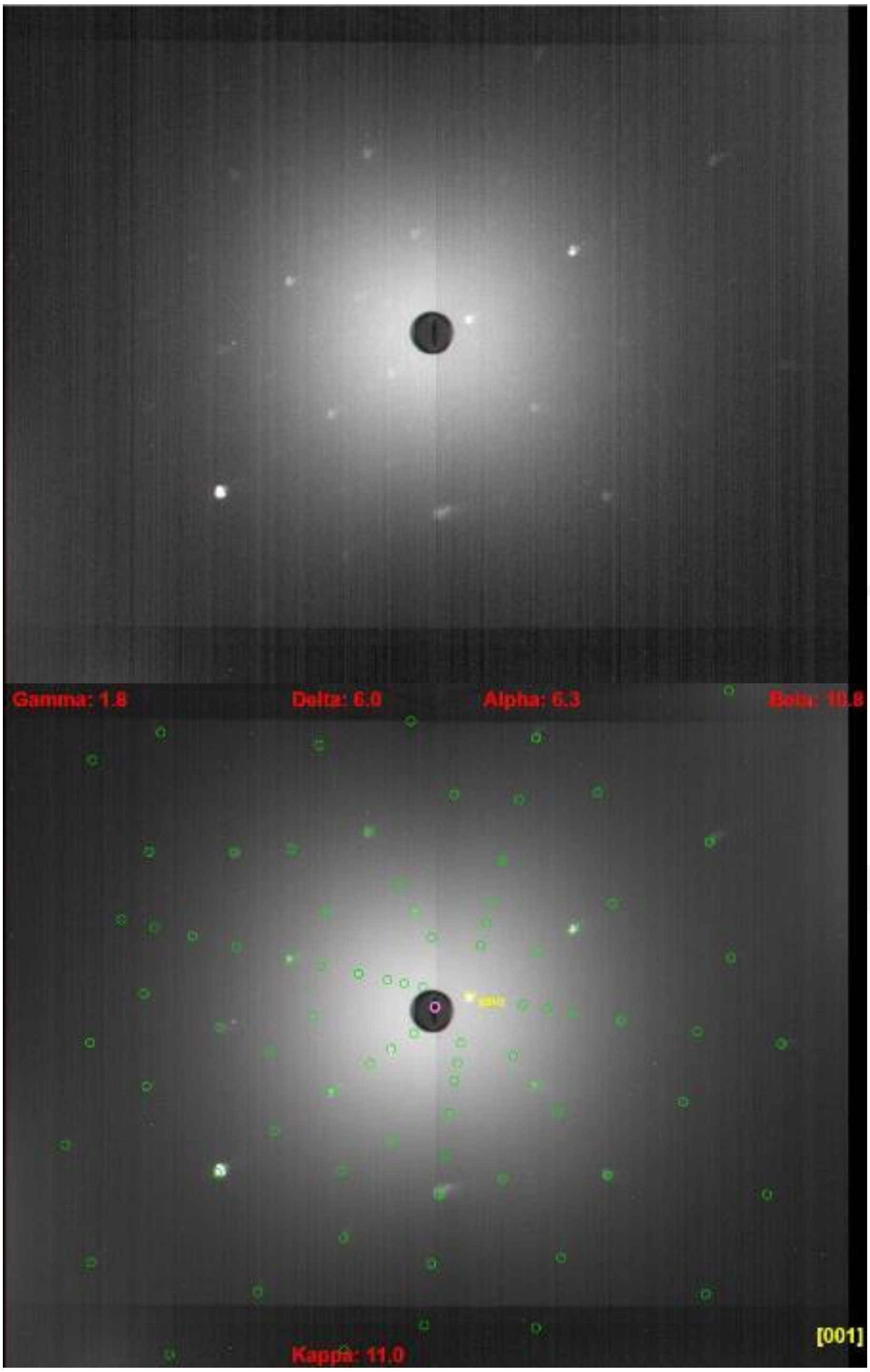

**Figure D.5 :** Laue pattern of test bar number 5.

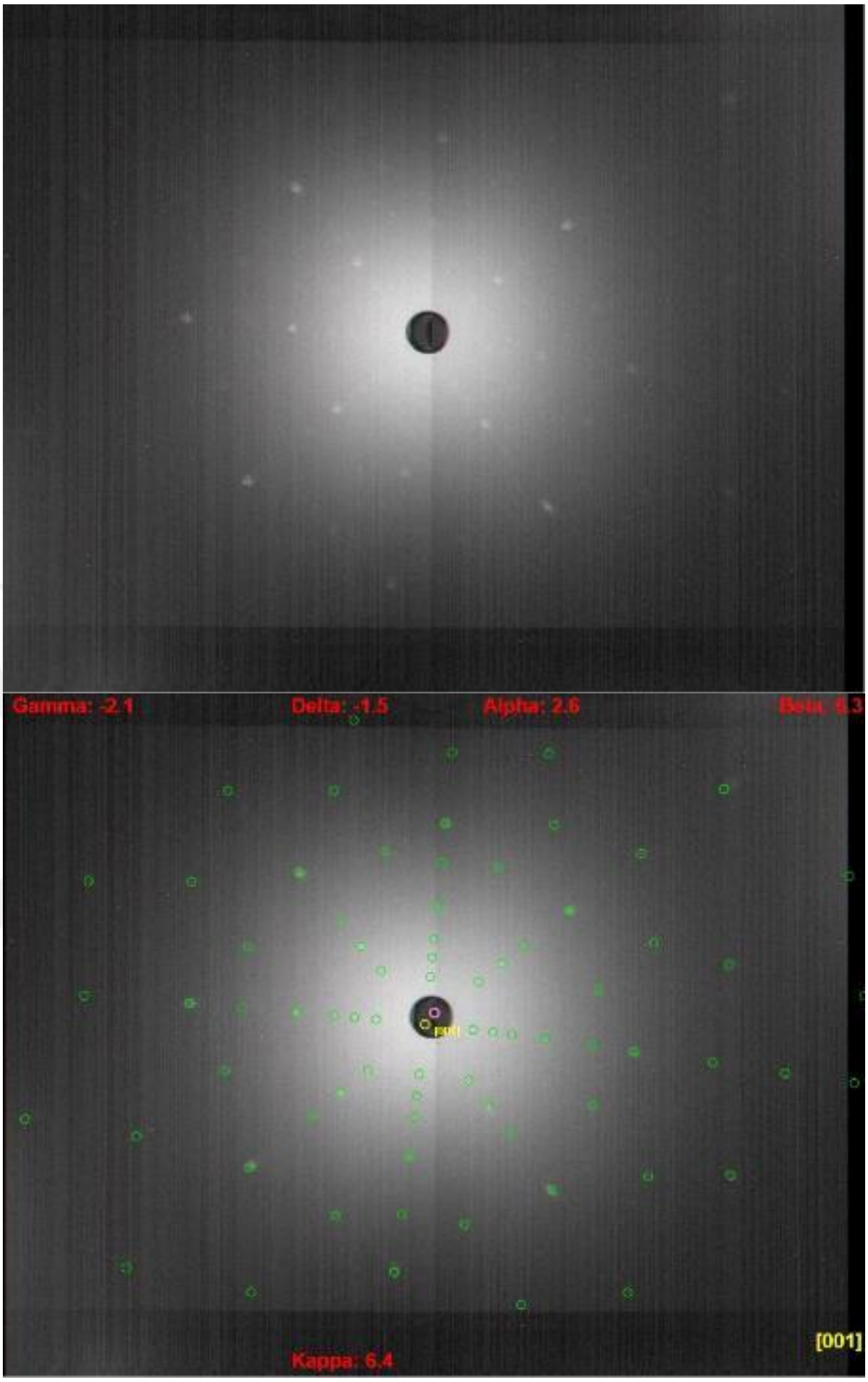

**Figure D.6 :** Laue pattern of test bar number 6.

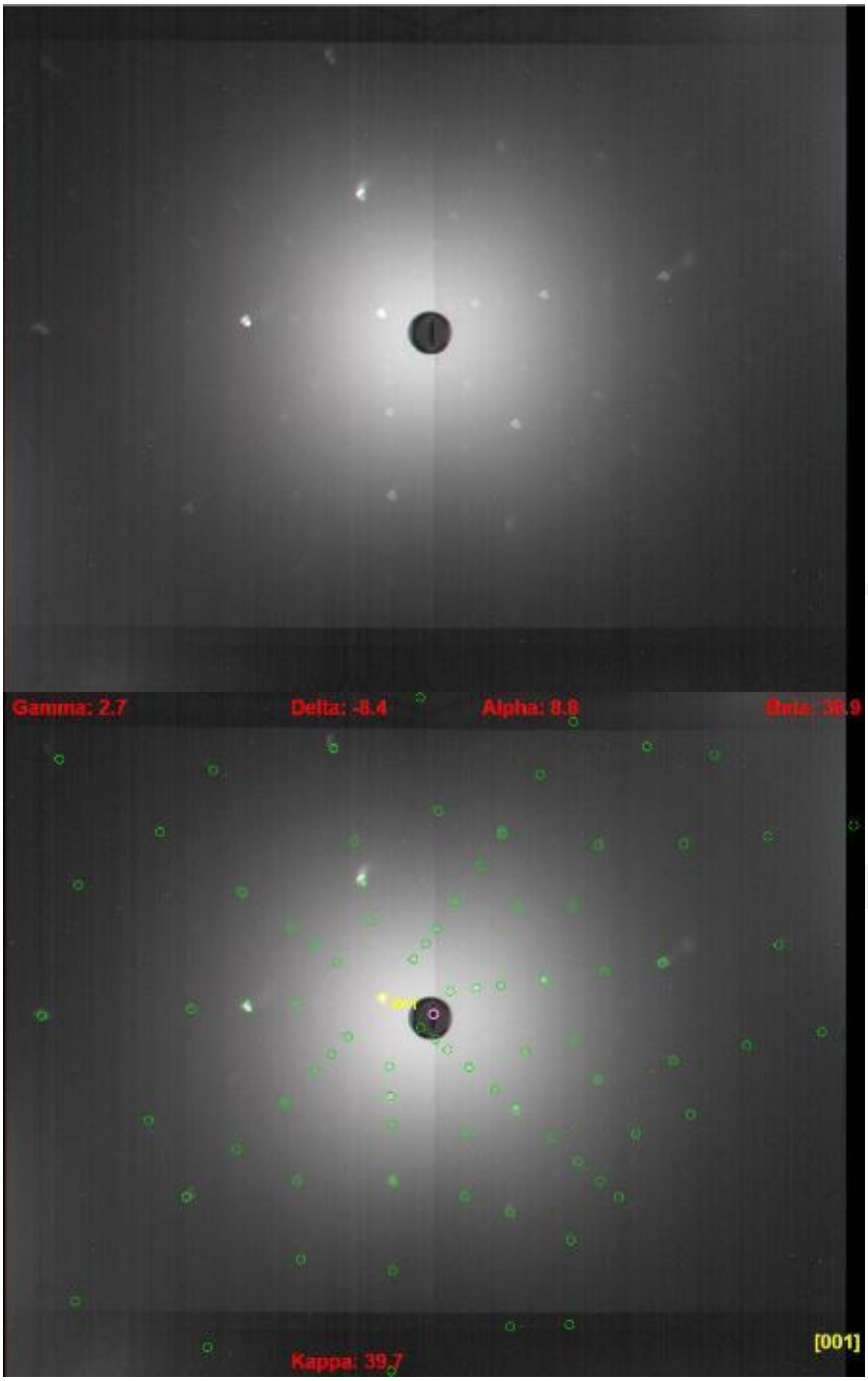

**Figure D.7 :** Laue pattern of test bar number 7.

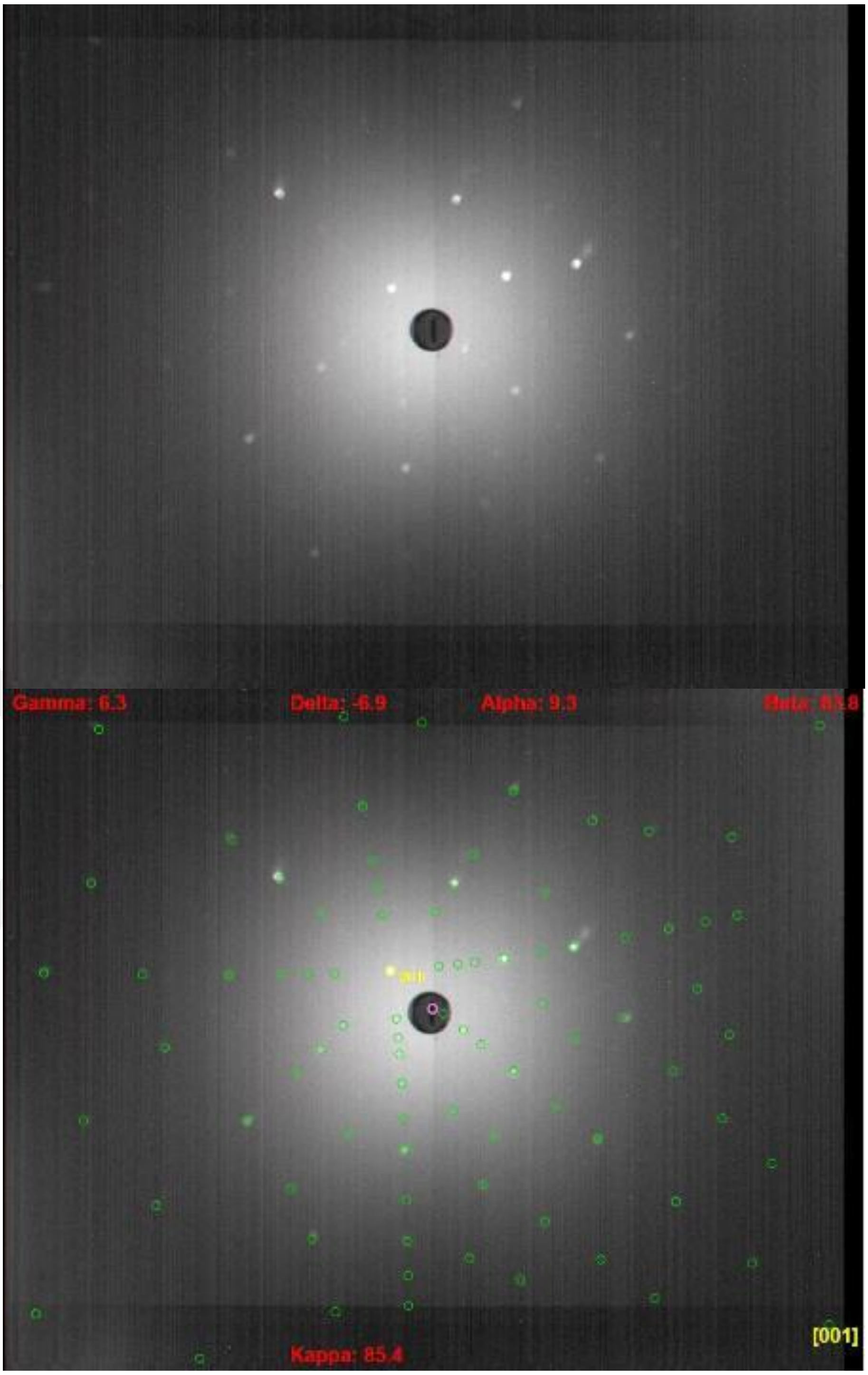

**Figure D.8 :** Laue pattern of test bar number 8.

**APPENDIX E** Stress-Strain Diagrams of the Samples

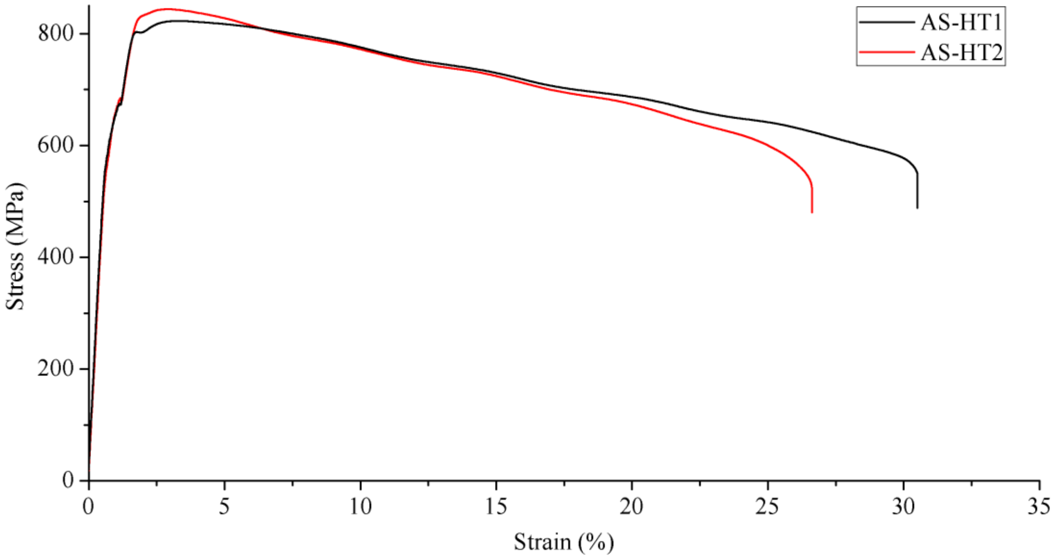

**Figure E.1 :** Stress-Strain diagrams of As-HT samples at 982ºC.

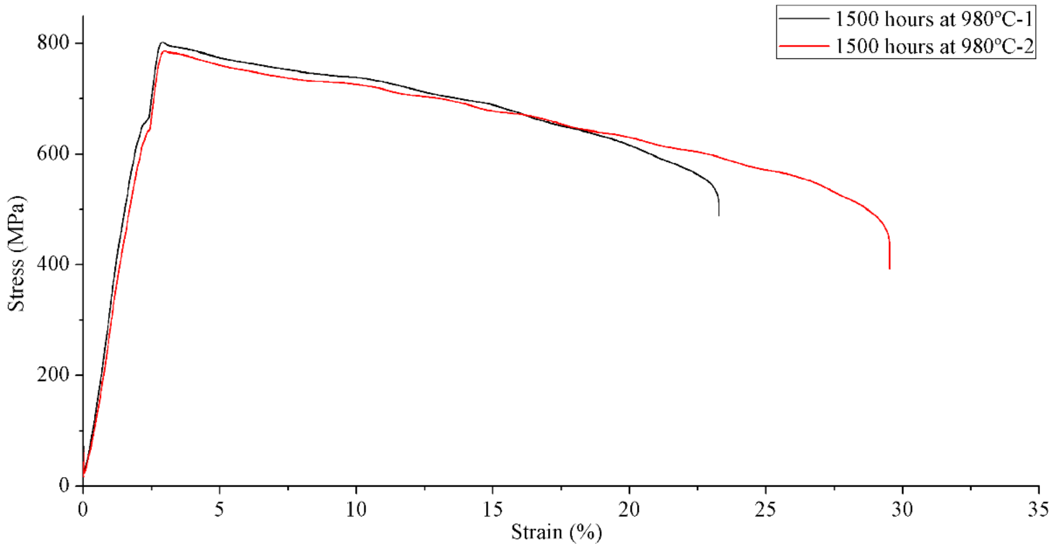

**Figure E.2 :** Stress-Strain diagrams at 982ºC of samples held for 1500 at 980ºC.

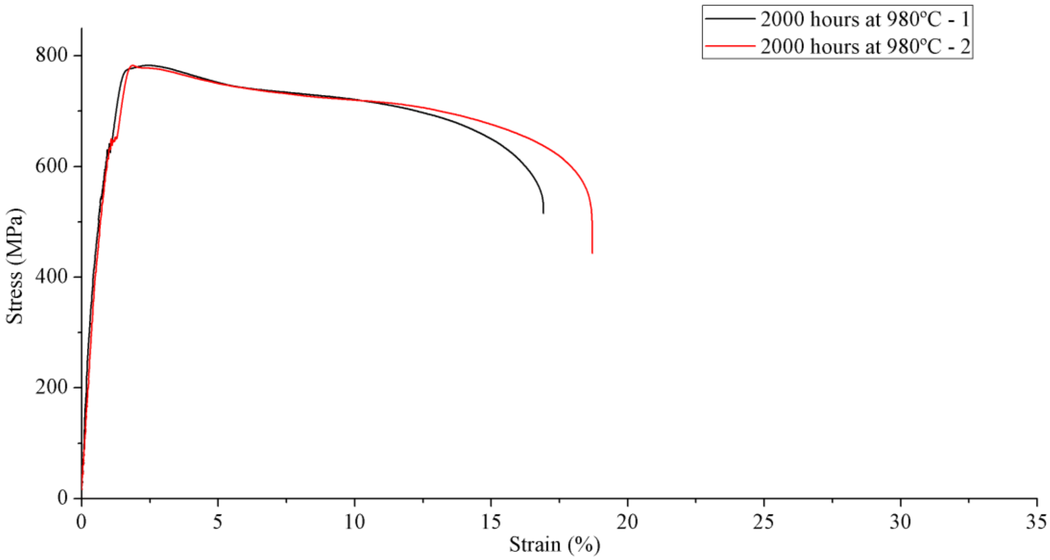

**Figure E.3 :** Stress-Strain diagrams at 982ºC of samples held for 2000 at 980ºC.

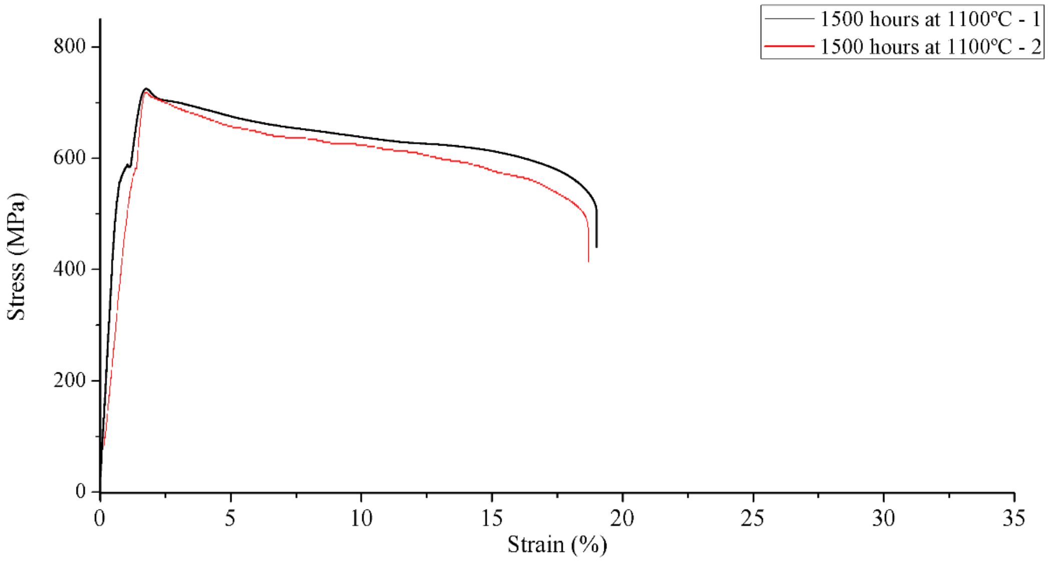

**Figure E.4 :** Stress-Strain diagrams at 982ºC samples held for 1500 at 1100ºC.

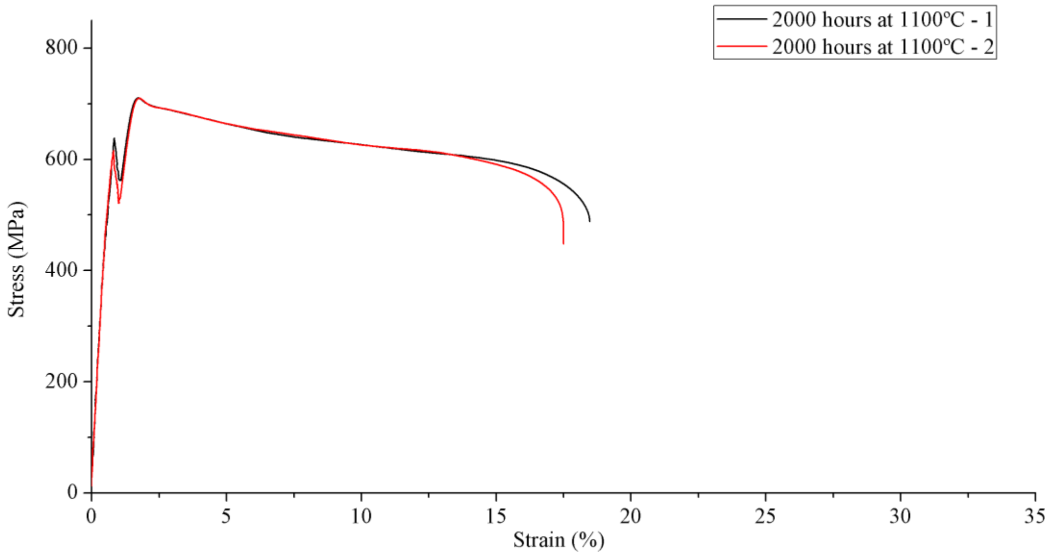

**Figure E.5 :** Stress-Strain diagrams at 982ºC samples held for 2000 at 1100ºC.

**APPENDIX F** Section View of Fractured Samples

**Figure F.1 :** Cracks on section view of the fractured AS-HT sample.

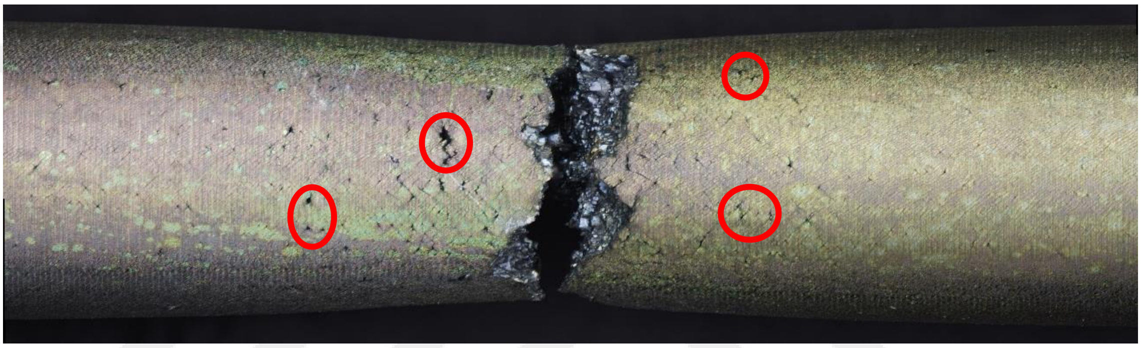

**Figure F.2 :** Cracks on section view of the fractured sample held for 1500 hours at 980ºC.

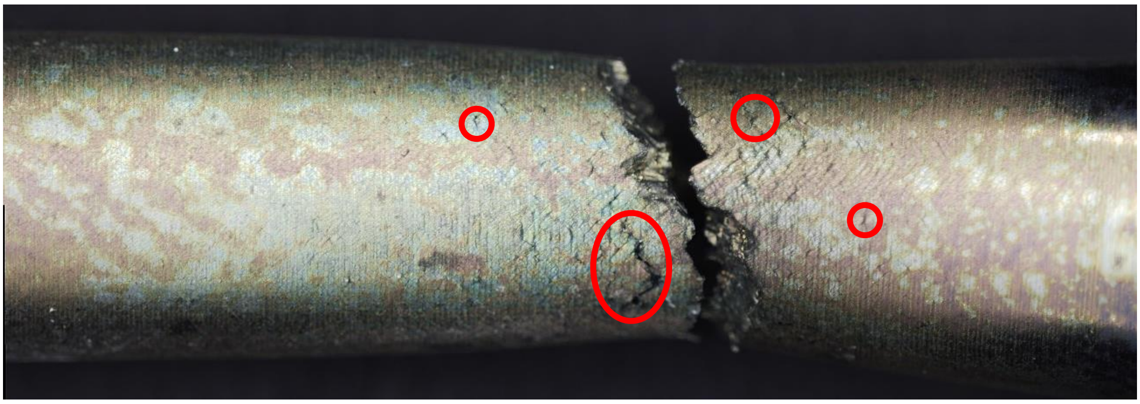

**Figure F.3 :** Cracks on section view of the fractured sample held for 2000 hours at 980ºC.

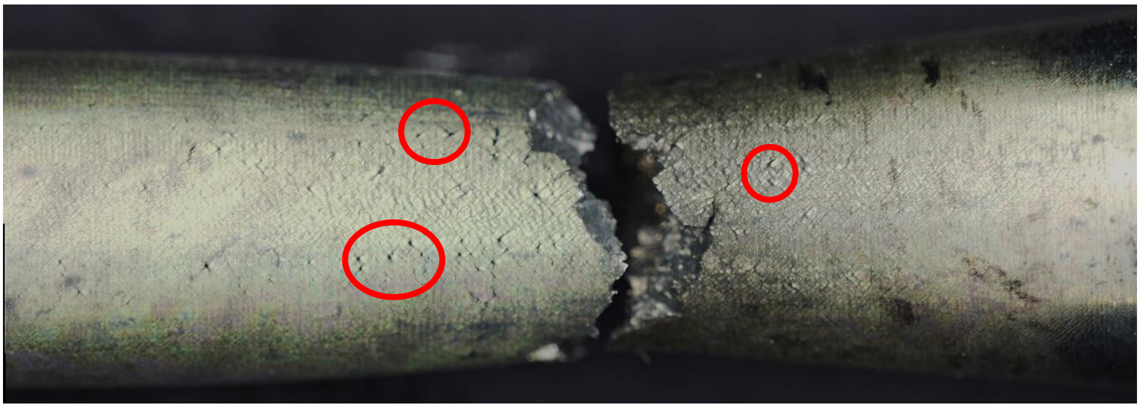

**Figure F.4 :** Cracks on section view of the fractured sample held for 1500 hours at 1100ºC.

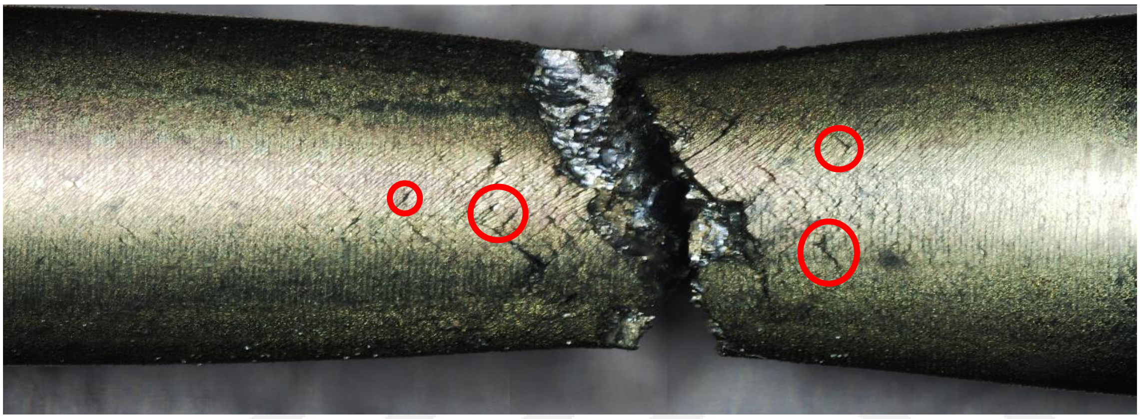

**Figure F.5 :** Cracks on section view of the fractured sample held for 2000 hours at 1100ºC.

# CURRICULUM VITAE

**Name Surname** **:** Sertaç ALPTEKİN

**EDUCATION** **:**

- **B.Sc.** **:** 2016, Middle East Technical University, Faculty of Engineering, Department of Metallurgical and Materials Engineering

**PROFESSIONAL EXPERIENCE AND REWARDS:**

- 2017- … Researcher at Materials Institute of TUBITAK Marmara Research Center